preprint

Daresbury Laboratory

DL/P 300E

A STUDY OF ELASTIC PHOTOPRODUCTION OF LOW MASS K^+K^- PAIRS FROM HYDROGEN IN THE ENERGY RANGE 2.8-4.8 GeV

by

D.P. BARBER, J.B. DAINTON, L.C.Y. LEE, R. MARSHALL, J.C. THOMPSON and D.T. WILLIAMS, Daresbury Laboratory;
T.J. BRODBECK, G. FROST, G.N. PATRICK, G.F. PEARCE, D. NEWTON and T. SLOAN, University of Lancaster;
G.R. BROOKES, W.J. HAYNES and P.B. WILKES, University of Sheffield.

Submitted to Z. Physik C.

OCTOBER 1981

Science and Engineering Research Council

DARESBURY LABORATORY

Daresbury, Warrington WA4 4AD

A Study of Elastic Photoproduction of Low Mass K^+K^- Pairs from Hydrogen in the Energy Range 2.8-4.8 GeV

D.P. Barber[1], J.B. Dainton[1], L.C.Y. Lee[2], R. Marshall[3],
J.C. Thompson[4] and D.T. Williams
Daresbury Laboratory
T.J. Brodbeck, G. Frost[5], G.N. Patrick[3], G.F. Pearce[1],
D. Newton and T. Sloan
University of Lancaster
G.R. Brookes, W.J. Haynes[4] and P.B. Wilkes[6],
University of Sheffield

Abstract

The results of an experiment to study elastic K^+K^- photoproduction are presented. Differential cross sections and spin density matrix elements for $\phi(1.019)$ production are studied as a function of incident photon energy and over a wide range of momentum transfer, t ($t_{min} > t > -1.5$ (GeV/c)^2). Helicity conserving amplitudes are observed to dominate ϕ production throughout this range and the differential cross sections exhibit a forward diffractive peak which cannot be understood in terms of a simple exponential dependence. A new value of the photon ϕ coupling constant is determined and shown to be consistent with e^+e^- annihilation measurements. A detailed study of the energy dependence of the differential cross sections is made, including other experimental data, and the extracted effective Regge trajectory compared with other diffractive processes. A study of the dependence of the K^+K^- decay angular distribution on invariant mass reveals evidence for an s wave contribution interfering with the p wave ϕ which may be attributable to the S^* meson.

Submitted to Z. Physik C

Present mailing addresses

1 DESY, 2000 Hamburg 52, Notkestrasse 85, Fed. Rep. of Germany.
2 University of London Computing Centre, 20 Guilford Street, London, UK.
3 Rutherford Laboratory, Chilton, Didcot, Oxon, UK.
4 CERN, 1211 Geneva 23, Switzerland.
5 MCS Division, Plessey Telecommunications Systems, Ltd., Maidenhead, U.K.
6 Daresbury Laboratory, Daresbury, Warrington, UK.

1. Introduction

The elastic photoproduction of K^+K^- pairs from protons is known to be dominated by the production of the $\phi(1.019)$ meson [1]. The ϕ production mechanism exhibits properties characteristic of a diffractive process, namely a peripheral forward peak in the differential cross-section $\frac{d\sigma}{dt}$ and a total cross-section which does not fall with increasing photon energy. Measurements of the ϕ spin polarisation out to $|t| \sim 0.3$ (GeV/c)^2 reveal a large contribution from production amplitudes which conserve s channel helicity [1]. Dominance of a diffractive production mechanism is to be expected because the application of the Okubo Zweig Iizuka (OZI) rule to the appropriate quark duality diagrams eliminates all baryon and meson exchange in the s and t channels respectively (to the extent that the ϕ is a pure $s\bar{s}$ quark antiquark state).

Combining data from existing experiments shows that $\frac{d\sigma}{dt}$ varies like $e^{\sim 5.6t}$ for $|t| < 0.4$ (GeV/c)^2 and $e^{\sim 4.2t}$ for $|t| > 0.4$ (GeV/c)^2 [2]. Such a change in logarithmic slope was confirmed in a single experiment and reported in a previous publication [3]. The dependence of $\frac{d\sigma}{dt}$ on incident photon energy k is found to be consistent with little shrinkage both for $|t| < 0.4$ (GeV/c)^2 using data with $3.0 < k < 6.7$ GeV [1] and for $|t| > 0.4$ (GeV/c)^2 by combining data from a number of experiments [2].

In the context of the vector dominance model (VDM) photons interact with hadrons via intermediate vector mesons. Interpretation of ϕ photoproduction in terms of the cross-section for elastic ϕp scattering and the photon-ϕ coupling constant, γ_ϕ, leads to the expression

$$\frac{d\sigma}{dt}(\gamma p \to \phi p) = \frac{\alpha}{4}\frac{4\pi}{\gamma_\phi^2}\frac{d\sigma}{dt}(\phi p \to \phi p)\left(\frac{q^*}{k^*}\right)^2 \qquad (1)$$

where α is the fine structure constant, q^* and k^* are the momenta of the incident photon and the ϕ respectively in the overall centre of mass system. The last term $\left(\frac{q^*}{k^*}\right)^2$ allows for the finite rest mass of the ϕ and is important near the ϕp threshold [4]. The additional so-called "diagonal" assumption

has also been made in which the inelastic scattering processes $\phi p \to \rho p$ and $\phi p \to \omega p$ are considered negligible.

Using the optical theorem, equation (1) yields an expression relating the ϕ photoproduction cross-section at t = 0 to the total ϕp interaction cross-section, $\sigma_T(\phi p)$:

$$\left(\frac{d\sigma}{dt}\right)_{t=0} (\gamma p \to \phi p) = \frac{\alpha}{64\pi} \frac{4\pi}{\gamma_\phi^2}(1 + \eta_\phi^2)\ \sigma_T^2(\phi p) \left(\frac{q^*}{k^*}\right)^2 \qquad (2)$$

where η_ϕ is the ratio of real to imaginary parts of the forward ϕp elastic scattering amplitude. Thus, in principle, knowledge of any two of $\frac{\gamma_\phi^2}{4\pi}$, $\sigma_T(\phi p)$ and η_ϕ permits a determination of the third.

Behrend et al. [1] have used their precise measurements of the energy dependence of $\left(\frac{d\sigma}{dt}\right)_{t=0}$ and equation (2) to study the correlation of $\sigma_T(\phi p)$ and $\frac{\gamma_\phi^2}{4\pi}$. They assume a value of -0.06 for η_ϕ determined by Bartalucci et al. [5] from a measurement of ϕ interference with the Bethe-Heitler process in wide angle e^+e^- pair production. For a value of $\frac{\gamma_\phi^2}{4\pi}$ of 2.83±0.2 determined from e^+e^- annihilation [6] they find $\sigma_T(\phi p)$ is 9.6±0.3 mb which is compatible with naive quark model predictions [7].

A study of the mass dependence of the photoproduced K^+K^- decay distribution has revealed a significant mass dependent asymmetry below the ϕ peak which is inconsistent with pure ϕ decay [8]. An understanding of this result in terms of interference between s and p K^+K^- partial waves is acceptable and can be interpreted successfully as interference between longitudinal (helicity 0) ϕ and S^* ($J^P = 0^+$) photoproduction.

In this paper we present in detail the results of a study of elastic K^+K^- photoproduction. In section 2 we give a description of the experimental procedure and in section 3 the method of selecting events for the reaction

$$\gamma p \to K^+K^-p \qquad (3)$$

In section 4 we describe the analysis methods used to extract the differential cross sections and spin density matrix elements for ϕ photoproduction. Section 5 contains the elastic ϕ photoproduction measurements in the energy range $2.8 < k < 4.8$ GeV, expanding the results given in our previous publication [3]. Further details are contained in [9]. We study the s and t dependence of the differential cross sections over the t range, $t_{min} > t > -1.5$ $(GeV/c)^2$. From extrapolations of these measurements to t = 0 we study the correlations between $\gamma_\phi^2/4\pi$ and $\sigma_T(\phi p)$ and between $\gamma_\phi^2/4\pi$ and η_ϕ using equation (2) with assumed values for the third variable. Together with measurements from other experiments we discuss the properties of the "effective Pomeron" Regge pole in the t channel and compare with high energy measurements of pp elastic scattering. In addition the ϕ spin density matrix elements are used to discuss briefly the reaction production mechanism. Section 6 describes the measured mass dependence of the statistical tensors of the K^+K^- decay distribution which are used to provide evidence for s-p wave interference below the ϕ peak. An interpretation in terms of K^+K^- s wave interference with helicity 0 ϕ photoproduction is given and used to extract estimates for the S^* photoproduction cross section. Section 7 presents our conclusions.

2. Experimental Method

The data presented here formed part of the LAMP2 experimental programme to study multi-particle final states from photoproduction reactions using the 5 GeV electron synchrotron NINA at Daresbury. Fig. 1 shows a diagram of the apparatus, further details of which have already been published [10,11]. The 5 GeV electron beam was converted in a photon tagging system into a bremsstrahlung beam with a tagged energy range of 2.8 to 4.8 GeV. The photon beam was focussed, by focussing the

electron beam, to a spot of diameter 1 cm (containing 95% of the flux) at a 30 cm long liquid hydrogen target with a cell diameter of 2.5 cms. Immediately downstream of the hydrogen target was a large aperture magnetic spectrometer (W75) containing 7 multiwire proportional chambers (MWPC), 6 of which were located within the magnetic field volume and one of which was located at the downstream exit of the magnet. These MWPC's were used for detection and momentum analysis of charged tracks. Covering the exit aperture of the magnet a scintillation counter hodoscope (BHBV) acted as a charged particle trigger counter, and a 480 element lead glass detector (Pb Glass) was situated further downstream to detect and trigger on photons and electrons which traversed the magnet. A strip scintillation counter, V, was placed in the median plane of the magnet exit aperture to veto the copious production of e^+e^- pairs.

The trigger for the experiment was either at least one charged particle traversing the whole spectrometer or a deposition of energy (> 500 MeV) in the lead glass, (the latter trigger was not used for this experiment but was used to study reactions with π^o production), in coincidence with an interacting tagged photon. Non-interacting beam photons were vetoed in a small lead glass counter (G) placed downstream of the whole apparatus. Halo beam photons were vetoed upstream of the apparatus in a lead scintillator sandwich (H) with a 2.5 cm diameter hole through which the beam passed. The single charged particle trigger used for the results presented here permitted sensitivity over a large range of t for elastic K^+K^- photoproduction with finite acceptance over the whole range of the decay angular distribution.

3. Data reduction

The data were taken in four separate experimental runs during which a total of 10.7 million triggers were accumulated of which 9.1 million

satisfied the charged particle trigger. Events with two charged tracks of opposite sign in the spectrometer and with a reconstructed vertex within the volume of the liquid hydrogen target were selected as K^+K^- candidates. After these criteria had been applied 2.9% of the charged particle triggers survived, the majority of which were $\pi^+\pi^-$ pairs. The good energy resolution of both the tagging system (6-11 MeV error on the tagged photon energy) and the spectrometer permitted a kinematic identification of events of reaction (3) in the ϕ region of the K^+K^- mass distribution. The two particles in each event were assumed to be a K^+ and K^- and the invariant mass of the pair was calculated. The recoil mass M_x in the process

$$\gamma p \rightarrow K^+K^-X$$

was also calculated using the incoming photon energy and the momenta of the K^+K^- particles. A scatter plot of M_{KK}^2 versus M_x^2 for a sample ($\sim$ 40%) of the data is shown in fig. 2. The elastic ϕ signal can be clearly seen as a concentration at $M_{KK}^2 \sim 1.04$ $(GeV/c^2)^2$ and $M_x^2 \sim 0.88$ $(GeV/c^2)^2$, i.e. at the ϕ and proton mass squared respectively. The horizontal band at $M_x^2 \sim 0.65$ $(GeV/c^2)^2$ is due to misidentified pions from the process $\gamma p \rightarrow \pi^+\pi^-p$.

Events were selected as candidates for reaction (3) if the recoiling mass from the K^+K^- pair was in the range $0.857 < M_x < 1.02$ GeV/c^2, i.e. consistent with the proton mass within the known experimental resolution. A further cut was made to the data to eliminate any remaining e^+e^- pairs; any event was rejected if the energy deposited in the lead glass for either track was consistent with the momentum of the track measured in the magnetic spectrometer (to within 3 standard deviations using the known resolution of the lead glass detector [11]). This led to a measured loss of 2% of the good events due to hadrons depositing all their energy in the lead glass for which appropriate normalisation corrections were made.

Fig. 3(a) shows a histogram of M_{KK} for events satisfying these selection criteria and fig. 3(b) shows the same histogram for events rejected as e^+e^- pairs. A clear elastic ϕ signal is observed with a small background due to misidentified $\pi^+\pi^-$ pairs and non-resonant K^+K^- pairs in fig. 3(a), with no significant signal in the sample rejected as e^+e^- pairs in fig. 3(b).

4. Methods used in the Data Analysis

To obtain the differential cross sections and decay angular distributions of the K^+K^- pairs, corrections for the apparatus acceptance and for kaon decay in flight were necessary. The acceptance was finite throughout the K^+K^- decay angular range for the t range studied. Therefore weighting of events by the reciprocal of the apparatus efficiency adequately corrected calculations of the production cross sections and decay distributions. An event weight was calculated in two stages, first an acceptance weight was obtained and then a reconstruction weight. The acceptance weight corrected for the effects of aperture and trigger biases. The reconstruction weight corrected for losses in the pattern recognition and kinematics programmes, particularly from distortion of reconstructed track momenta due to K decays in flight.

The reconstructed events were read into a Monte Carlo programme one at a time. Each defined a point in the five-dimensional space of photon energy k, momentum transfer t, K^+K^- mass M_{KK} and K^+K^- decay angles $\cos\theta$ and ϕ at which the experimental acceptance was required. 100 Monte Carlo events were generated for each of these values of k, M_{KK}, t, $\cos\theta$ and ϕ but with interaction vertex and azimuth about the beam chosen at random. Each of the K^+ and K^- mesons were then tracked through the spectrometer by Runge-Kutta integration, and all K decay modes simulated. The tracks were finally propagated to the trigger hodoscope to test if the trigger

had been satisfied. The coordinates of the track hits at each proportional chamber plane were converted to wire numbers by assuming that the nearest wire to the coordinate would register a hit [12]. For those Monte Carlo events satisfying the aperture cuts and trigger requirements the wire addresses were written onto a magnetic tape in the same format as the raw data. At the end of the 100 Monte Carlo events the acceptance weight, given by the ratio of trials to successes, was also written onto tape.

To calculate the reconstruction weight the events from this subsidiary magnetic tape were read into a second programme. Proportional chamber inefficiencies were simulated and the surviving hits were then passed through the pattern recognition and momentum reconstruction programme. The surviving events were then subjected to the same kinematic analysis and cuts which had been applied to the data. In this way the apparatus resolution was simulated and the loss of events outside the proton mass cut ($\sim$ 22%) was measured. The reconstruction weight was obtained from the ratio of trials to successes and the total event weight obtained from the product of the acceptance and reconstruction weights. Fig. 4(a) shows a spectrum of the acceptance weights and fig. 4(b) a spectrum of the reconstruction weights for one experimental run.

The cross sections were calculated in a bin of k and t from

$$\frac{d\sigma}{dt} = F \frac{\sum W_n}{n \, \Delta t . R} \qquad (4)$$

where $\sum W_n$ is the sum of the weights of all events in the bin, R is the branching ratio $\phi \to K^+K^-$ (0.486), Δt is the width of the t bin and F is the luminosity of the experiment in the k bin. The incident beam flux was measured by counting the coincidence rate between tagged photons and the lead glass beam veto counter G.

The following corrections were then made to this flux:

1) dead time and random effects $\sim$ 2%

ii) photon losses due to pair production in the target and MWPC chamber material $\sim 3\%$

iii) liquid hydrogen density in the target: the e^+e^- cross section from a Cu target was found to agree with the QED prediction whereas the measured cross section from H_2 was found to be 7% lower than QED; we therefore deduced that the actual hydrogen density in our experiment was 7% lower than that calculated from the temperature and pressure monitors on the target;

iv) loss of $K^\pm$ mesons due to interactions in the target and spectrometer material ($\sim 3\%$);

v) trigger scintillation counter inefficiences ($\lesssim 3\%$).

The K^+K^- decay distribution was studied using a method of moments in the s and t channel helicity frames. In both frames a right-handed coordinate system was used with the y axis perpendicular to the ϕp production plane. In the rest frame of the ϕ the z axis was taken to be antiparallel to the direction of the recoil proton for the s channel analysis and parallel to the direction of the incident photon for the t channel analysis. In both cases the K^+ was taken to be the decay indicator.

For events in a selected range of k, t and K^+K^- mass, the decay distribution in angles $\Omega = (\cos\theta,\phi)$ for the K^+ is written

$$I(\Omega) = \sum_{L=0}^{2J} \sum_{M=-L}^{L} t_{LM}\, Y^*_{LM}(\Omega) \qquad (5)$$

where t_{LM} are the statistical tensors of the distribution, parameterising the spin, parity and spin polarisation structure of the K^+K^- system. The t_{LM} are averaged over the range of k, t and mass in each bin. From the orthonormality of the $Y_{LM}(\Omega)$ functions

$$t_{LM} = \frac{\int I(\Omega)\, Y_{LM}(\Omega)\, d\Omega}{\int I(\Omega)\, d\Omega}$$

The statistical tensors were estimated from the data using

$$t_{LM} = \langle Y_{LM} \rangle = \frac{\sum_n W_n Y_{LM}(\Omega_n)}{\sum_n W_n} \qquad (6)$$

Because (5) is real, that is because the generalised density matrix of the K^+K^- system is Hermitian, and because of parity invariance in the production mechanism

$$t_{L-M} = (-1)^M t^*_{LM}$$

and

$$\mathrm{Im}\, t_{LM} = 0 \quad .$$

The measurement of the imaginary parts of the statistical tensors can be used to ensure that we have eliminated systematic biases due to experimental apparatus by checking that they are consistent with zero. In all that follows the t_{LM} are assumed real.

If we assume that the K^+K^- pairs are dominated by p wave production, the ϕ spin density matrix elements $\rho^{\ell\ell'}_{mm'}$ can be related to these moments

$$\mathrm{Re}\ \rho^{11}_{10} = \sqrt{4\pi}\ \sqrt{\tfrac{5}{3}}\ \tfrac{1}{2}\ t_{21}$$

$$\rho^{11}_{1-1} = -\sqrt{4\pi}\ \sqrt{\tfrac{5}{6}}\ t_{22} \qquad (7)$$

and

$$\rho^{11}_{00} - \rho^{11}_{11} = \sqrt{4\pi}\ \sqrt{5}\ \tfrac{1}{2}\ t_{20} \quad .$$

In addition we use the normalisation given by the trace of the p wave density matrix

$$\rho^{11}_{00} + 2\rho^{11}_{11} = 1 \qquad (8)$$

In practice, the spin projected differential cross sections were determined from the data

$$\rho^{\ell_1\ell_2}_{m_1m_2} \frac{d\sigma}{dt} = \frac{F}{\Delta t R}\left[\alpha^{\ell_1\ell_2}_{m_1m_2} \sum_{n\ \mathrm{events}} Y_{LM}(\theta_n,\phi_n) W_n\right] \qquad (9)$$

where the $a^{\ell_1\ell_2}_{m_1m_2}$ are the multiples of $\sqrt{\pi}$ given in equation (7). Dividing by the values of $\frac{d\sigma}{dt}$ obtained from equation (4) then allowed the $\rho^{\ell_1\ell_2}_{m_1m_2}$ to be determined. In section 5 we discuss the necessary corrections due to the background under the ϕ signal.

To study the K^+K^- mass dependence of the moments we used unnormalised moments defined by

$$s_{LM} = \frac{F}{\Delta M} \sum_{n \text{ events}} W_n Y_{LM}(\theta_n, \phi_n) \qquad (10)$$

where ΔM is the bin width in mass. The unnormalised s_{LM} and normalised t_{LM} moments are related by

$$s_{LM} = \frac{d\sigma}{dM} t_{LM} \qquad (11)$$

where $\frac{d\sigma}{dM}$ is the production cross section as a function of K^+K^- mass for events in a given range of t.

5. Study of Elastic ϕ Photoproduction

5.1 Correction for background

Fig. 5 shows the mass spectrum for events identified by recoil invariant mass as consistent with reaction (3) for one experimental run ($\sim$ 40% of the data). Fig. 5 also shows the result of a fit of the spectrum to a cubic polynomial background together with a ϕ line shape generated by a Monte Carlo programme which included the smearing due to experimental resolution. A fit with a linear background was also made and this gave nearly the same χ^2 as the cubic function. We conclude that a linear parametrisation represents the background adequately which thus can be subtracted by taking slices of the mass spectrum on each side of the ϕ peak.

The correction for the background under the ϕ mass peak was made by using the control regions marked A and B in fig. 5. In each bin of k and t the cross section and spin-projected cross sections were calculated from equations (4) and (9) for the background in regions A and B and for the signal plus background in the ϕ peak. Subtracting the average of regions A and B then gave the ϕ production cross sections.

5.2 The t dependence of the ϕ production cross section

The t variation of the differential cross section, $\frac{d\sigma}{dt}$, for elastic ϕ photoproduction is summarised in Table I and shown in fig. 6. The cross sections are presented in figs. 6(a) for the photon energy ranges $2.8 \leq k < 3.8$ GeV and $3.8 \leq k < 4.8$ GeV. A difference in slope between the small t ($|t| < 0.4$ (GeV/c)^2) and large t ($|t| > 0.4$ (GeV/c)^2) cross sections is apparent; a fit over the entire t range to the form e^{Bt} gives a χ^2 probability of only 2%. Furthermore, there is possible structure in the region $0.25 \lesssim |t| \lesssim 0.4$ (GeV/c)^2. Fig. 6(b) shows $\frac{d\sigma}{dt}$ averaged over the complete photon energy range where the structure is revealed with greater significance.

The change of slope from the small $|t|$ to the large $|t|$ region seems to be a common feature of reactions dominated by Pomeron exchange. The effect has been seen previously in studies of elastic K^+p, π^+p and $p^\pm p$ scattering between 10 and 14 GeV where the slope parameter for $|t| \lesssim 0.2$ (GeV/c)^2 is 1-2 units larger than for $0.2 \lesssim |t| \lesssim 0.5$ (GeV/c)^2 [13]. At higher energies, ($460 < s < 2900$ GeV^2), Barbiellini et al [14] observe a change in the slope of the t distribution in elastic pp scattering at $|t| \sim 0.1$ (GeV/c)^2. Also there is evidence for a steeper slope at small t in ρ photoproduction [15].

5.3 The total cross section for elastic ϕ photoproduction

The total cross sections were obtained by integrating the differential cross sections over the measured t range. The values obtained are shown in Table I. They are higher than those of Behrend et al [1] probably because our measurements at large t are higher than the small t extrapolation; i.e. it is a consequence of the change in the slope.

5.4 Energy dependence of the ϕ production cross section at small $|t|$ values

The variation of $\frac{d\sigma}{dt}$ for $|t| < 0.25$ (GeV/c)^2 over the three incident photon energy regions, $2.8 \leq k < 3.4$, $3.4 \leq k < 4.0$ and $4.0 \leq k < 4.8$ GeV, is presented in fig. 7 and Table II. Also shown are the small $|t|$

measurements of Behrend et al. [1] in approximately the same k intervals ($3.0 \leq k < 3.5$, $3.5 \leq k < 4.0$, and $4.0 \leq k < 4.8$ GeV). These data agree well with the present results except perhaps in the lowest energy region. The straight lines in fig. 7 are fits of the form

$$\frac{d\sigma}{dt} = \frac{d\sigma}{dt}\Big|_{t=0} e^{Bt} \qquad (12)$$

to our data only.

Fig. 8(a) shows the fitted values of $(\frac{d\sigma}{dt})_{t=0}$ and fig. 8(b) the values of the slope parameter B together with the results of other experiments as a function of photon energy. With the exception of Behrend et al. [1] all previous experiments had only limited data at small $|t|$ and relied on extrapolating across a large t range. We therefore include in fig. 8(b) only measurements with data in the region $|t| < 0.4$ $(GeV/c)^2$.

Fig. 8 shows clearly that $(\frac{d\sigma}{dt})_{t=0}$ increases with energy. Recently measurements of the total ϕ photoproduction cross sections [19] have been made which show an increase with energy between 30-180 GeV. This would indicate that $(\frac{d\sigma}{dt})_{t=0}$ should continue to rise with energy beyond the range shown in fig. 8(a). The smooth curve in fig. 8(a) shows a fit of the form

$$(\frac{d\sigma}{dt})_{t=0} = \beta(\frac{q_\phi^*}{k^*}) \qquad (13)$$

to the data. We assume here that equation (2) will be a good parameterisation of the data, neglecting the change of $\sigma_T(\phi p \to \phi p)$ with energy, which should be small over the energy range of fig. 8(a). The best fit to the data from this experiment gave $\beta = 3.10 \pm .32$ $\mu b/(GeV/c)^2$ with a confidence level of 93.9%. As can be seen from fig. 8(a) the resulting curve rises sharply from threshold ($k = 1.57$ GeV) and becomes less energy dependent with increasing k, thus providing an adequate parameterisation of all existing data below an incident energy of 10 GeV. This curve is in good agreement with the fit of Behrend et al. [1] which gave $\beta = 2.93 \pm 0.08$ $\mu b/(GeV/c)^2$. By fitting the present measurements combined with the data of reference [1]

the result $\beta = 3.02 \pm 0.08$ $\mu b/(GeV/c)^2$ was obtained (C.L. = 56.9%).

Equation (2) shows that the correlation between $\gamma_\phi^2/4\pi$, $\sigma_T(\phi p \to \phi p)$, and η_ϕ makes it impossible to determine uniquely these parameters from the fitted value of β. However, by assuming a quark model prediction of 10 mb for $\sigma_T(\phi p)$, the curve shown in fig. 9(a) was obtained for the variation of $\gamma_\phi^2/4\pi$ and η_ϕ. Alternatively, if η_ϕ^2 is assumed negligible, the correlation between $\gamma_\phi^2/4\pi$ and $\sigma_T(\phi p)$ can be plotted as in fig. 9(b).

If $\sigma_T(\phi p \to \phi p) = 10$ mb and $\eta_\phi \approx 0$, the result $\gamma_\phi^2/4\pi = 3.0 \pm 0.5$ is obtained. This is insensitive to the value of η_ϕ for $0 > \eta_\phi > -.3$ which covers the probable range of values [5]. This result is in agreement with the values for e^+e^- annihilation experiments and with the analysis of Behrend et al. [1].

5.5 The effective Regge trajectory

The possible shrinkage of $\frac{d\sigma}{dt}$ indicated in the previous section was examined more closely across the whole t range by calculating an effective Regge trajectory $\alpha(t)$. Two different fits were made, each involving different assumptions about the Regge amplitude:

1) The s dependence of the differential cross section in each bin of t was fitted to the form

$$\frac{d\sigma}{dt} = \beta(t)\ s^{2\alpha(t)-2} \qquad (14)$$

where $\beta(t)$ is the Regge residue function. The fit was performed in the same three bins of k as in section 5.3 with $\alpha(t)$ and $\beta(t)$ as free parameters. The values of $\alpha(t)$ obtained are shown in fig. 10. A linear fit to the data in fig. 10 gives

$$\alpha(t) = (0.82 \pm .21) + (0.71 \pm .63)t$$

The dashed line in fig. 10 comes from a fit to pp scattering data [16] (see below).

2) A simultaneous fit was performed to both the s and t dependences of the differential cross-sections using equation (14), in which $\alpha(t)$ was assumed to be a linear function of t and $\beta(t)$ to be an exponential function. Table III shows the different forms of the functions used and the results of the fits. To obtain higher precision and for comparison with other experiments the results from this experiment were combined with other published data. For $|t| < 0.4$ (GeV/c)^2 the high statistics data of reference [1] were used and for $|t| > 0.4$ (GeV/c)^2 the SLAC results [25,26] were included. Where appropriate the cross sections from these experiments were renormalised to a common branching ratio for $\phi \to K^+K^-$ of 0.486.

To obtain satisfactory parameterisations, it was necessary to fit the small $|t|$ ($|t| < 0.4$ (GeV/c)^2) and large $|t|$ ($|t| > 0.4$ (GeV/c)^2) regions separately. In the case of the small $|t|$ data, a satisfactory fit could not be obtained if the lowest energy data of reference [1] were included, due to the apparent steep t dependence of this particular measurement (see fig. 7). The fits in Table III omitted the latter set of data which disagrees with our measurements.

The results of the two fits indicate that the small $|t|$ and large $|t|$ regions exhibit different degrees of shrinkage. A possible explanation of the phenomenon could be the two component model of the Pomeron described by Kane [17]. In this model a central component (conventional Pomeron) plus an additional peripheral contribution account for the small $|t|$ shrinkage in high energy pp scattering. The amplitudes for these contributions are of the form shown in fig. 11. The central contribution has a slow energy dependence, whilst the peripheral contribution shrinks rapidly and behaves in t space as a Bessel function, with its first zero around $|t| \sim 0.2$ (GeV/c)^2. As s increases, there is a region in $|t| \sim .5$ (GeV/c)^2 where the peripheral contributions cross for different s values, and therefore display only a weak energy dependence. Perhaps this effect contributes to the structure in $\frac{d\sigma}{dt}$ at $|t| \sim 0.4$ (see fig. 6).

It is interesting to note the quark model sum-rule prediction of Gotsman and Levy [18] for the Pomeron trajectory. They substituted experimental cross sections for elastic hadron scattering in the relation

$$\frac{d\sigma}{dt}(\phi p \to \phi p) = \left[\left(\frac{d\sigma}{dt}(K^+p)\right)^{\frac{1}{2}} + \left(\frac{d\sigma}{dt}(K^-p)\right)^{\frac{1}{2}} - \left(\frac{d\sigma}{dt}(\pi^-p)\right)^{\frac{1}{2}}\right]^2 \qquad (15)$$

and then fitted the resulting predictions to the Regge form of equation (14). By assuming a linear trajectory, the result

$$\alpha(t) = (0.86 \pm 0.03) + (0.25 \pm 0.05)t$$

was obtained for data in the energy range 8-40 GeV and t range $0.3 < |t| < 0.7$ (GeV/c)^2. This indicates shrinkage, and is consistent with the parameterisation obtained here.

However, the behaviour of pp elastic scattering seems to be somewhat different from that observed in this experiment. In fig. 10 the dashed line shows the effective Pomeron trajectory from the fit of Collins et al. [16] to pp scattering data in the energy range $21 < s < 2860$ GeV^2. The agreement between the $\gamma p \to \phi p$ and pp trajectories appears to be poor, particularly at small $|t|$ where the ϕ data shows a greater energy dependence. It has been noted by Dass and Praas [20] that if the Pomeron is a pure pole, $\alpha(t)$ should be the same in both $\gamma p \to \phi p$ and high energy elastic pp scattering. However, if Regge cuts are present, $\alpha(t)$ would, in general, be different due to the different ways in which the cuts affect the amplitudes of each reaction.

5.6 ϕ Spin Density Matrix and the Reaction Production Mechanism

The results of the ϕ polarisation analysis described in section 4 are presented in figs. 12 and 13, which show the t and k dependence of the density matrix elements in the s channel helicity frame. The data are consistent at all t and k with helicity conservation in the s channel

although without knowledge of the incident photon polarisation this does not constitute definite proof. In particular there is no evidence for any significant helicity non-conservation for $|t| > 0.4$ (GeV/c)^2. This is to be contrasted with ρ^o photoproduction [26] where substantial deviations occur for $|t| > 0.4$. There is no evidence for any dependence of the ϕ spin polarisation on incident photon energy k in our energy region.

In figs. 14 and 15 we plot the ϕ density matrix evaluated in the t channel helicity frame. As is to be expected there are significant discrepancies from helicity conservation in this frame away from the forward direction where the s and t channel frames no longer coincide.

We have adopted the approach of Randa [21] in order to conclude in a model independent manner as much as possible about the ϕ photoproduction mechanism in our energy range. Randa proposes calculation of the ratio

$$\delta = \frac{\max(g_1 g_2)}{A}$$

where A is the average magnitude of those amplitudes which will be large for a certain hypothesis, and g_1 and g_2 are the maximum magnitudes of the different possible small amplitudes whose presence would violate the hypothesis. For example if the hypothesis is helicity conservation at the photon-ϕ vertex, then g_1 and g_2 are the maximum magnitudes of single helicity and double helicity flip amplitudes.

Table IV summarises the results of applying the lower bounds on δ derived by Randa for three hypotheses, helicity conservation at the photon vertex, helicity conservation at both the photon and proton vertices and helicity conservation at both vertices together with t channel naturality (to leading order in t/s). We average the ϕ spin density matrix over two ranges of t, $|t| > 0.4$ and $|t| < 0.4$ (GeV/c)^2. At small $|t|$ there is consistency with the three hypotheses tried to within about 1 standard deviation, that is δ differs from zero by no more than about one error. At large $|t|$ the consistency is good to within about 1½ standard deviations.

Nowhere is there evidence for significant violation of the assumptions made.

In fig. 12 we show superimposed on the ϕ spin density matrix the predictions of the amplitude analysis of Behrend et al. [1] for $|t| < 0.22$ (GeV/c)^2. The model dependent assumptions made are described in detail in Derado et al. [22]. Elastic ϕ photoproduction is assumed to be dominated by natural parity exchange (in the limit of small t/s) and the t dependences of all Regge residue functions are taken to be the same, determined by the overall t dependence of $\frac{d\sigma}{dt}$. The exchange naturality assumption constrains $|\text{Re } \rho^{11}_{10}|$ to be small; however the model fails to account for ρ^{11}_{1-1} at larger $|t|$. The discrepancy can be traced to a (relatively) large and negative prediction of the photon double helicity flip amplitude $f_{-1\frac{1}{2}1\frac{1}{2}}$ for $|t| > 0.22$ (GeV/c)^2 which interferes constructively with the dominant helicity conserving amplitude $f_{1\frac{1}{2}1\frac{1}{2}}$ in the amplitude analysis of reference [1].

We conclude that in our energy range the dynamics of elastic ϕ photoproduction are consistent with simple diffraction in which helicity conservation and natural parity exchange dominate from the forward region out to $|t|$ of 1.3 (GeV/c)^2. The change of logarithmic slope and the possible structure of $\frac{d\sigma}{dt}$ at $|t| \sim 0.4$ (GeV/c)^2 need not be associated with a radical change in this production mechanism and appears to be a property of the diffractive process in this reaction.

6. Study of s wave K^+K^- Photoproduction

In this section the results of the mass dependent moments analysis (integrated over k and t) are presented. The unnormalised moments s_{LM} were calculated using equation (10). In fig. 16 we show such moments for $L \leq 2$ and in fig. 17 the cross section $\frac{d\sigma}{dM}$ plotted as a function of $M_{K^+K^-}$. In fig. 16(a) only the moments s_{20} and s_{10} are inconsistent with zero throughout the mass range studied. The former is due to the strong

ϕ signal which is produced mainly by a mechanism conserving s channel helicity (as shown in section 5.5). We argue that the structure seen in the s_{10} moment is due to an s-p wave interference in the K^+K^- system. There are, however, two possible alternatives to this hypothesis:

a) A misunderstood bias in the apparatus which has not been properly corrected.

b) A background due to kinematically misidentified events from inelastic $\pi^+\pi^-$ photoproduction (see fig. 2).

In fig. 16(b) we show the imaginary parts of the unnormalised moments. These are all consistent with zero, indicating, as discussed in section 3, that the experimental biases are well understood. Thus alternative (a) is unlikely. We also consider alternative (b) to be unlikely on the grounds that there are no known narrow J = 0 or J = 1 resonances which decay to $\pi^+\pi^-$ of the mass required to produce the observed structure.

We therefore conclude that there is a significant s wave contribution near threshold in the K^+K^- system which is manifest through its interference with the helicity zero p wave amplitude. Moreover the mass dependence of the interference, a rapid variation near the $\phi(1.019)$ mass, suggests that the latter is associated with ϕ production. It therefore follows that in our photon energy range s channel helicity is not exactly conserved in $\phi(1.019)$ photoproduction, as suggested in section 5.5 and in the amplitude analysis of [1].

We have attempted to understand the observed s_{10} by assuming that in the mass range of interest the K^+K^- helicity zero, isospin zero, p wave amplitude a_p^o is saturated by $\phi(1.019)$ production. a_p^o is thus written as a relativistic Breit-Wigner [23] with the known ϕ mass and width. For the isoscalar s wave amplitude, a_s, we have assumed either an s wave Breit-Wigner or a simple non-resonant amplitude with mass dependence $1/M_{KK}$ and with no intrinsic phase variation.

The unnormalised spherical harmonic moment s_{10} is related to a_s and a_p^o by

$$s_{10} = \frac{1}{\sqrt{\pi}} \sum_{|\Delta\lambda|=0,1} \mathrm{Re}\left[a_s^* |\Delta\lambda| a_p^o |\Delta\lambda|\right] \qquad (16)$$

if we assume parity invariance in the K^+K^- production mechanism. The additional index $|\Delta\lambda|$ is the helicity flip (0 or 1) of the proton for each value of which there is an s and a p wave K^+K^- amplitude. In the forward direction ($t=t_{min}$) angular momentum conservation demands that $|\Delta\lambda| = 1$ for meson production in the helicity substate 0; we have assumed like Fries et al. [8] that only such proton helicity flip amplitudes contribute significantly to s_{10} throughout the t range of the data, i.e. that there is only a single a_s and a_p^o to extract from the data. If $a_{s|\Delta\lambda|=0}$ was finite in this t range then s_{11} would also exhibit a large asymmetry due to interference with the dominant helicity conserving ϕ production amplitude $a^1_{p|\Delta\lambda|=0}$. Thus we can write

$$s_{10} = \frac{1}{\sqrt{\pi}} \mathrm{Re}\left[a_s^* \, a_p^o\right] \qquad (17)$$

Both a_s and a_p^o have a contribution to their phases from production so that s_{10} depends on the relative production phase δ of a_s and a_p^o. We assume also that δ is not dependent on K^+K^- invariant mass.

Normalising the amplitude a_s and a_p^o to the total photoproduction cross sections of s and p wave K^+K^- pairs, σ_s and σ_p^o respectively, we have fitted the measured s_{10} and $\frac{d\sigma}{dM}$ of figs. 16 and 17 to determine σ_s, σ_p^o and δ using equation (16). In order to parameterise any background due to $\pi^+\pi^-X$ in both S_{10} and $\frac{d\sigma}{dM}$ we have included a smoothly varying contribution to the latter with constant t_{10} over the fitted K^+K^- mass range. Then a simultaneous fit to $\frac{d\sigma}{dM}$ and s_{10} not only determined any slowly varying background but also checked that our understanding of experimental resolution was correct. In all that follows the total

ϕ photoproduction cross section to K^+K^- was assumed to be 226±9 nb as measured in our photon energy range (section 5).

In Table V we summarise the details of the fits assuming a resonant or a non-resonant a_s. In both cases a single unique solution was found which was independent of the magnitude and choice of shape for the $\pi^+\pi^-X$ background in $\frac{d\sigma}{dM}$ and of its contribution to s_{10} within the errors on the extracted parameters. In addition the mass and width of the S* found in the resonance fit are consistent with the published values [24].

Like Fries et al. [8] we find that the hypothesis of an S* resonance in the K^+K^- s wave is a good description of the observed asymmetry. An S* production phase near 90^o relative to $\phi(1.019)$ production is favoured suggesting a non-diffractive production mechanism if all ϕ production (both $\lambda = 1$ and $\lambda = 0$) is diffractive. The observed mass dependence of s_{10} is relatively insensitive to the choice of S* mass between threshold and the ϕ mass. In fig. 17 we show $\frac{d\sigma}{dM}$ and s_{10} determined by the best fit superimposed on the data together with the S* and $\pi\pi X$ background contributions.

The hypothesis of the non-resonant threshold enhancement for a_s also provides a numerically acceptable fit to the data. In order to reproduce the structure observed in the dependence of s_{10} on mass a rather large K^+K^- s wave signal is required together with a large contribution to s_{10} from the small (in intensity) $\pi\pi X$ background (fig. 17(b)). The relatively small contribution of the $\pi\pi X$ background to the observed spectrum would imply either that the background outside the recoil proton mass region of fig. 2 contains a large fraction of K^+K^-X inclusive production or that there is a sudden reduction of the $\pi\pi X$ signal correlated exactly with the elastic K^+K^-P region. We consider both possibilities to be unlikely and therefore favour the resonant solution. However, with the statistical precision of these data we are unable to reject the hypothesis quantitatively.

From the parameterisation of s_{10} as interference between the S* and $\phi(1.019)$ we find a total S* photoproduction cross section to K^+K^- in our

energy range of 96±20 nb. This must be taken as an upper limit in view of the fact that there exists the possibility of a significant non-resonant admixture to a_s. The total ϕ photoproduction cross section in helicity substate 0 (with proton helicity flip) is found to be 17.4±8.1 nb, that is about 8±4% of the total production cross section, if S* production dominates a_s.

Fries et al. [8] quote an upper limit of 2.7±1.5 nb for S* production assuming the spin density matrix element ρ^{11}_{00} of the ϕ is 0.03±0.015 and σ_p is 250±20 nb in their photon energy range between 4.6 and 6.7 GeV. We have fitted their published statistical tensor s_{10} to our amplitudes assuming the experimental resolution quoted in Behrend et al. [1] and the S* parameters of Table V. The results are presented in Table V and yield an upper limit for S* production of 10.2±6.1 nb. The discrepancy between our determination of the S* cross-section and that of Fries et al. [8] using their data can possibly be traced to either a factor of π omitted in their equation (5a) or a missing square root in reference [9] of their paper or different S* resonance parameters. There remains a suggestion that σ_s may decrease with incident photon energy, which is to be expected for non-diffractive production. It will thus be interesting to see if the s wave K^+K^- signal under the $\phi(1.019)$ persists at higher incident photon energy.

7. Conclusions

Using a tagged photon beam and large aperture magnetic spectrometer we have studied forward and wide angle elastic K^+K^- photoproduction.

In the elastic photoproduction of $\phi(1.019)$ between 2.8 and 4.8 GeV incident photon energy we have observed that:

1) The differential production cross-section $\frac{d\sigma}{dt}$ exhibits a decrease in logarithmic slope at $t \sim -0.4$ $(GeV/c)^2$. There is evidence for structure in the t dependence of $\frac{d\sigma}{dt}$ in this region.

2) There is clear evidence from these and other data that $(\frac{d\sigma}{dt})_{t=0}$ rises with increasing incident photon energy.

3) The variation of the photon-ϕ coupling constant $\gamma_\phi^2/4\pi$ with η_ϕ and $\sigma_T(\phi p)$ is consistent with other elastic ϕ photoproduction experiments. If $0 \lesssim \eta_\phi \lesssim .2$ and $\sigma_T(\phi p)$ assumed to be 10 mb, then $\gamma_\phi^2/4\pi = 3.0 \pm 0.7$ which is in agreement with the measurements of e^+e^- annihilation in storage rings.

4) There is evidence for shrinkage of $\frac{d\sigma}{dt}$. At small t this shrinkage is greater than at large t. The effective Regge trajectory of these and other data is best parameterised as

$$\alpha(t) = (1.4 \pm 0.1) + (1.9 \pm 0.6)t \qquad |t| < 0.4$$
$$\alpha(t) = (1.1 \pm 0.1) + (0.5 \pm 0.2)t \qquad |t| > 0.4$$

which indicates that the Pomeron effective trajectory is still not well understood, particularly in ϕ photoproduction.

5) Model independent considerations of the ϕ spin density matrix show that the reaction mechanism is consistent to within about 1½ standard deviations with the expectations of simple diffraction, namely dominance of helicity conservation and natural parity exchange throughout the t range studied, $t_{min} > t > -1.3\ (GeV/c)^2$.

6) Between K^+K^- threshold and the ϕ mass, the K^+K^- decay distribution is observed to exhibit an asymmetry which can be interpreted as the production of s wave K^+K^- pairs. The assumption of $\phi(1.019)$ dominance of the p wave and S^* ($J^P=0^+$) dominance of the s wave, where the S^* is a resonance above threshold and below about 1.02 GeV/c^2 in K^+K^- mass, is found to give a good description of the mass dependence of the asymmetry. The relative production phase of each resonance is consistent with 90^o, expected if S^* production is non-diffractive. Although the resonant solution is qualitatively favoured, the hypothesis of a non-resonant s wave signal is also found to be numerically consistent with the data and the extracted S^* photoproduction cross section of 96±20 nb should therefore be taken as an upper limit in our energy range.

There is evidence from comparison with data at slightly higher energy to suggest a decreasing S^* photoproduction cross-section with increasing photon energy, as is to be expected if the production mechanism is non-diffractive.

We thank all our colleagues at Daresbury, Lancaster and Sheffield who have assisted in the LAMP2 project. We are grateful to Drs. E. Gabathuler and A.M. Osborne for their help in the early stages of the experiment. We should also like to thank Professors A. Ashmore, A.B. Clegg and W. Galbraith for their encouragement and support.

TABLE I

Differential and total cross sections averaged over

three ranges of incident photon energy

$\|t\|$ range $(GeV/c)^2$	$\frac{d\sigma}{dt}[\mu b/(GeV/c)^2]$		
	$2.8 \leq k < 3.8$ GeV	$3.8 \leq k < 4.8$ GeV	$2.8 \leq k < 4.8$ GeV
t_{min} - 0.05	1.780±0.264	1.723±0.287	1.752±0.195
0.05 - 0.10	1.406±0.198	1.257±0.159	1.332±0.127
0.10 - 0.15	1.046±0.139	0.845±0.119	0.946±0.091
0.15 - 0.20	0.942±0.120	0.747±0.095	0.844±0.077
0.20 - 0.25	0.669±0.103	0.574±0.096	0.621±0.070
0.25 - 0.030	0.393±0.102	0.391±0.078	0.392±0.064
0.30 - 0.35	0.552±0.097	0.324±0.068	0.438±0.059
0.35 - 0.40	0.680±0.103	0.410±0.072	0.545±0.063
0.40 - 0.45	0.494±0.104	0.381±0.080	0.437±0.066
0.45 - 0.50	0.360±0.101	0.233±0.061	0.297±0.059
0.50 - 0.60	0.433±0.079	0.184±0.035	0.314±0.043
0.60 - 0.70	0.174±0.090	0.196±0.049	0.185±0.051
0.70 - 0.80	0.019±0.080	0.156±0.038	0.169±0.044
0.80 - 0.90	0.010±0.081	0.062±0.034	0.089±0.044
0.90 - 1.0	0.165±0.066	0.101±0.033	0.133±0.037
1.0 - 1.10	0.105±0.062	0.101±0.039	0.093±0.036
1.10 - 1.20	0.024±0.057	0.054±0.033	0.035±0.033
1.20 - 1.30	0.059±0.054	0.052±0.028	0.053±0.030
1.30 - 1.40	0.039±0.049	0.013±0.034	0.026±0.030
1.40 - 1.50	-0.024±0.054	0.050±0.030	0.013±0.031
σ_T (μb)	0.472±0.029	0.415±0.021	0.440±0.018

TABLE II

Variation of the small $|t|$ differential cross section

with photon energy

$\|t\|$ range $(GeV/c)^2$	$\frac{d\sigma}{dt}[\mu b/(GeV/c)^2]$		
	$2.8 \leq k < 3.4$ GeV	$3.4 \leq k < 4.0$ GeV	$4.0 \leq k < 4.8$ GeV
t_{min} - 0.05	1.533±0.364	2.081±0.303	1.669±0.334
0.05 - 0.10	1.374±0.285	1.232±0.210	1.375±0.174
0.10 - 0.15	1.116±0.197	0.741±0.153	0.972±0.131
0.15 - 0.20	1.035±0.173	0.812±0.125	0.726±0.106
0.20 - 0.25	0.818±0.152	0.591±0.115	0.497±0.102

TABLE III

Simultaneous fits to the s and t dependence of the differential cross section

Fit	$\|t\|$ range $(GeV/c)^2$	α_o	α'	χ^2/DF	C.L.(%)
$Ae^{Bt}s^{2(\alpha_o+\alpha' t-1)}$	< 0.4	1.43±0.08	1.95±0.56	137/119	12
	≥ 0.4	1.15±0.12	0.62±0.18	58/73	90
$Ae^{Bt+Ct^2}s^{2(\alpha_o+\alpha' t-1)}$	< 0.4	1.41±0.08	1.77±0.58	136/118	12
	≥ 0.4	1.09±0.10	0.51±0.14	55/72	93
$Ae^{Bt+Ct^2+Dt^3}s^{2(\alpha_o+\alpha' t-1)}$	< 0.4	1.42±0.08	1.85±0.59	129/117	21
	≥ 0.4	1.09±0.11	0.53±0.16	55/71	93

NOTE: The higher energy data from SLAC[25,26] has been included in fits for $|t| \geq 0.4$ $(GeV/c)^2$, and the data from DESY/Karlsruhe[1] included in the fits for $|t| < 0.4$ $(GeV/c)^2$.

TABLE IV

Lower limits on δ, the ratio of largest violating amplitude to average conserving amplitude, in differing hypotheses for elastic φ photoproduction

hypothesis	lower limits on δ		
helicity conservation at photon vertex	$\delta \geq \sqrt{\frac{\rho_{00}}{2\rho_{11}}}$	$\delta \geq \frac{\|\rho_{1-1}\|}{4\rho_{11}}$	$\delta(1+\frac{\delta}{2}) \geq \frac{\|Re\rho_{10}\|}{2\rho_{11}}$
$\|t\| < 0.4$	0.17±0.15	0.01±0.01	0.0 ±0.01
$\|t\| > 0.4$	0.35±0.21	0.03±0.04	0.02±0.04
helicity conservation at both vertices	$\delta \geq \sqrt{\frac{\rho_{00}}{4\rho_{11}}}$	$\delta(1+\frac{\delta}{\sqrt{2}}) \geq \frac{1}{2\sqrt{2}}\frac{\|\rho_{1-1}\|}{\rho_{11}}$	$\delta(1+\frac{3\delta}{\sqrt{2}}) \geq \frac{1}{\sqrt{2}}\frac{\|Re\rho_{10}\|}{\rho_{11}}$
$\|t\| < 0.4$	0.12±0.11	0.01±0.01	0.0±0.02
$\|t\| > 0.4$	0.25±0.15	0.04±0.06	0.02±0.05
Helicity conservation at both vertices + natural parity exchange	$\delta \geq \sqrt{\frac{\rho_{00}}{8\rho_{11}}}$	$\delta(1+3\delta) \geq \frac{\|\rho_{1-1}\|}{2\rho_{11}}$	$\delta(1+7\delta) \geq \frac{\|Re\rho_{10}\|}{\rho_{11}}$
$\|t\| < 0.4$	0.09±0.08	0.01±0.02	0.01±0.02
$\|t\| > 0.4$	0.18±0.11	0.05±0.07	0.03±0.05

TABLE V

S* resonance production (this experiment)

M_ϕ GeV	Γ_ϕ GeV	M_S^2 GeV^2	$M_S\Gamma_S$ GeV^2	σ_p^o nb	σ_s nb	δ^o	$\langle Y_{10}\rangle_{\pi\pi}$	χ^2/d.f.
1.019	.004	1.002 ±.016	.044 ±.012	17.4 ±8.1	96.2 ±20.0	74 ±28	-0.0106 ±0.0112	11/14

non-resonance s wave threshold production (this experiment)

M_ϕ GeV	Γ_ϕ GeV	σ_p^o nb	σ_s nb	δ^o	$\langle Y_{10}\rangle_{\pi\pi}$	χ^2/d.f.
1.019	.004	3.6 ±2.0	10.2 ±4.1	1.0 ±20.0	-0.120 ±0.04	11/16

S* resonance production (data from [8])

M_ϕ GeV	Γ_ϕ GeV	M_S^2 GeV^2	$M_S\Gamma_S$ GeV^2	σ_p^o nb	σ_s nb	δ^o	χ^2/d.f.
1.019	.004	1.002	.0044	7.5	10.2 ±6.1	90	12/5

References

[1] H.J. Behrend et al., Nucl. Phys. B114 (1978) 22.

[2] M.A.R. Kemp and R. Marshall, Daresbury Laboratory report DL/P226 (1975).

[3] D.P. Barber et al., Phys. Lett. 79B (1978) 150.

[4] V. Barger and R.J.N. Phillips, Phys. Lett. 58B (1975) 197.

[5] S. Bartalucci et al., Nuovo Cim. 39A (1977) 374.

[6] D. Benaskas et al., Phys. Lett. B39 (1972) 289
Phys. Lett. B42 (1972) 507
Phys. Lett. B40 (1972) 685
Phys. Lett. B48 (1972) 155.

[7] From simple quark additivity and the quark content of π, K and φ mesons and of the nucleon many relations can be derived between φp and $K^\pm p$, $\pi^\pm p$, $K^\pm n$ and $\pi^\pm n$ total cross sections. An example is the result $\sigma_T(\phi p) = 2\sigma_T(K^+p) + \sigma_T(\pi^-p) - 2\sigma_T(\pi^+p)$.

[8] D.C. Fries et al., Nucl. Phys. B143 (1978) 408.

[9] G.N. Patrick, Ph.D. Thesis, University of Lancaster (unpublished).

[10] D.P. Barber et al., Nucl. Inst. Method. 155 (1978) 353.

[11] D.P. Barber et al., Nucl. Inst. Meth. 145 (1977) 453.

[12] It was proved by studying the residuals for straight tracks that the nearest wire to a track was the most probable wire to register a hit; for details see [10].

[13] R.K. Carnegie et al., Phys. Lett. 59B (1975) 313.

[14] G. Barbiellini et al., Phys. Lett. 39B (1972) 663.

[15] D.W.G.S. Leith, "Diffractive Photoproduction" in "Electromagnetic Interactions of Hadrons" Vol.I, edited by A. Donnachie and G. Shaw (Plenum Press, N.Y. 1978).
D.P. Barber et al., to be published.

[16] P.D.B. Collins, F.D. Gault and A. Martin, Nucl. Phys. B80 (1974) 135.

[17] G. Kane, "Implications of Experimental Data for our View of the Pomeron", Michigan report UM-73-10 (1973).

[18] E. Gotsman and A. Levy, Phys. Rev. D13 (1970) 3036.

[19] P.M. Egloff et al., Phys. Rev. Letters 43 657 (1979).
D. Aston et al., Nucl. Phys. B172 (1980) 1.

[20] G.V. Dass and H. Fraas, Annals of Physics 115 (1978) 467.

[21] J. Randa, Journal Phys. G. 3 (1977) 761.

[22] I. Derado et al., Nucl. Phys. B38 (1972) 541.

[23] J.D. Jackson, Nuvo. Cim. 34B (1964) 1644.

[24] C. Bricman et al., Phys. Lett. 75B (1978) 1.

[25] R.L. Anderson et al., Phys. Rev. D1 (1970) 27.
R.L. Anderson et al., Phys. Rev. D7 (1973) 3150.

[26] J. Ballam et al., Phys. Rev. D7 (1973) 3150.

[27] Aachen-Bonn-Hamburg-Heidelberg-Munchen Collaboration, Phys. Rev. 175 (1968) 1669.

[28] H. Alvensleben et al., Phys. Rev. Letters 28 (1972) 66.

[29] Ch. Berger et al.,Phys. Letts. 39B (1972) 659.

[30] H.J. Besch et al., Nucl. Phys. B70 (1974) 257.

Figure Captions

1. Plan view of the apparatus.

2. Scatter plot of recoil invariant mass squared against M^2_{KK} assuming the reaction $\gamma p \to K^+K^-X$ for events with two identified charged hadron tracks.

3. K^+K^- invariant mass spectrum for one experimental run.
   (a) $\gamma p \to K^+K^-p$ candidates with e^+e^- contamination removed,
   (b) candidates identified as electrons in the lead glass.

4. Histograms of the event weights (a) acceptance weights,
   (b) reconstruction weights for one experimental run.

5. The K^+K^- invariant mass spectrum fitted by a p wave Breit-Wigner line shape, smeared by experimental resolution with a cubic polynomial background. Regions A and B were used to estimate the background under the ϕ.

6. (a) $\frac{d\sigma}{dt}$ as a function of -t in two different photon energy ranges.
   (b) $\frac{d\sigma}{dt}$ as a function of -t averaged over the complete photon energy range.

7. Variation of $\frac{d\sigma}{dt}$ versus -t at small t at different incident photon energies.

8. Energy dependence of (a) $(\frac{d\sigma}{dt})_{t=0}$ and (b) the slope parameter B obtained from the fits in fig. 7. Key: • this experiment, ▲ ref. [1], □ ref. [26], x ref. [25], ◁ ref. [25], o ref. [27], Δ ref. [28], ∇ ref. [29], + ref. [30].

9. Variation of $\frac{\gamma_\phi^2}{4\pi}$ with (a) η_ϕ assuming $\sigma_T(\phi p) = 10$ mb and (b) $\sigma_T(\phi p)$ assuming $\eta_\phi = 0$.

10. Effective Regge trajectory extracted from fits to the s dependence of the differential cross sections. The dashed line is the Pomeron trajectory extracted from a fit [16] to high energy pp scattering data.

11. Schematic amplitudes in the two component model of the Pomeron.

12. ϕ spin density matrix elements in the s channel helicity frame as a function of -t. The smooth curves are from the amplitude analysis of reference [1].

13. ϕ spin density matrix elements in the s channel frame as a function of photon energy k.

14. ϕ spin density matrix elements, evaluated in the Gottfried-Jackson frame, as a function of -t.

15. Density matrix elements in the Gottfried-Jackson frame as a function of photon energy k.

16. (a) The unnormalised moments $s_{\ell m}$ in the s channel frame as a function of K^+K^- mass.

    (b) The imaginary parts of the unnormalised moments as a function of K^+K^- mass.

17. (a) $\frac{d\sigma}{dM}$ and s_{10} as a function of K^+K^- mass. The dashed curve shows the fitted $\pi\pi X$ background, the dash-dot curve shows the fitted sum of the assumed S^* signal plus the $\pi\pi X$ background, the solid curve shows this with the fitted ϕ signal added.

    (b) The same data with the fitted background assumed to be from non resonant s wave K^+K^- production rather than S^* production.

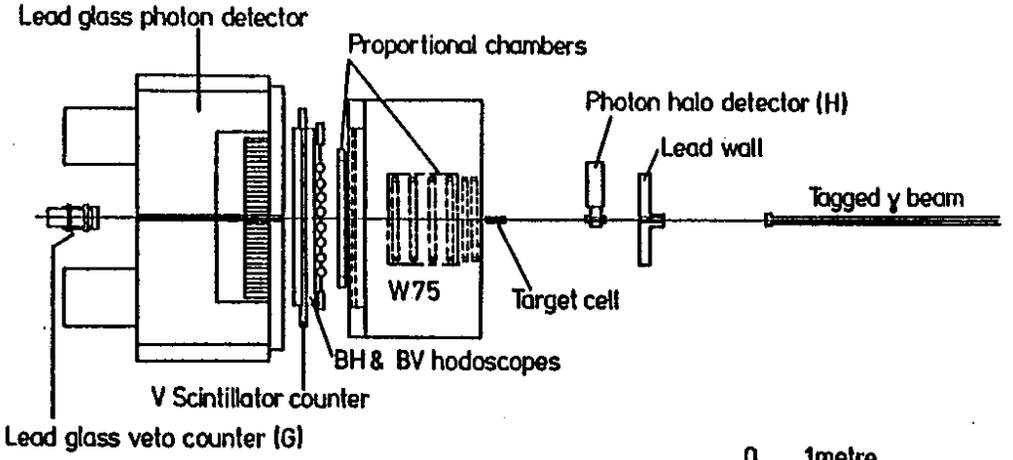

Fig. 1

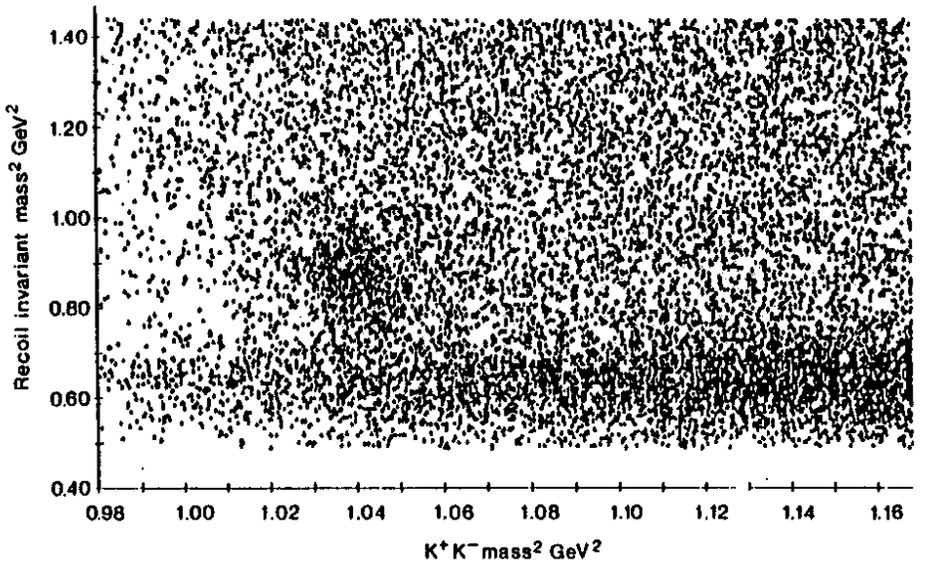
Recoil invariant mass² GeV²
1.40
1.20
1.00
0.80
0.60
0.40
0.98
1.00
1.02
1.04
1.06
1.08
1.10
1.12
1.14
1.16
K⁺K⁻ mass² GeV²

Fig. 2

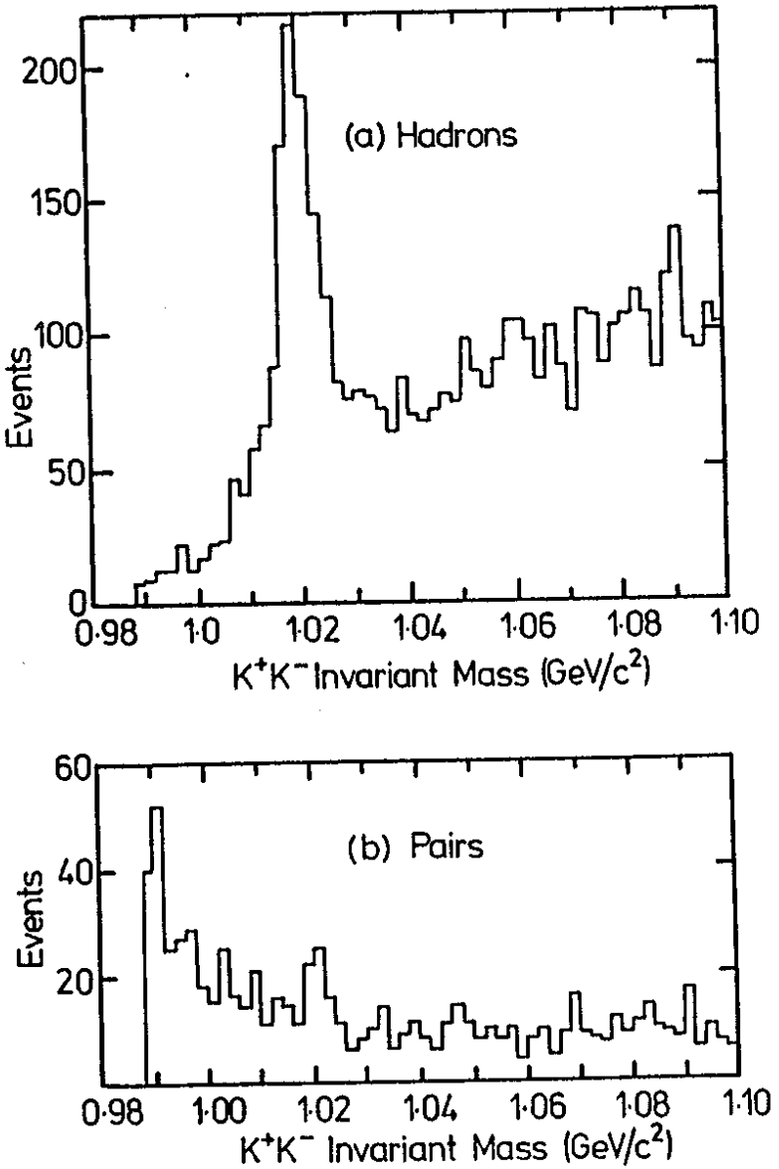
(a) Hadrons
Events
200
150
100
50
0
0·98
1·0
1·02
1·04
1·06
1·08
1·10
K⁺K⁻ Invariant Mass (GeV/c²)
(b) Pairs
Events
60
40
20
0·98
1·00
1·02
1·04
1·06
1·08
1·10
K⁺K⁻ Invariant Mass (GeV/c²)

Fig. 3

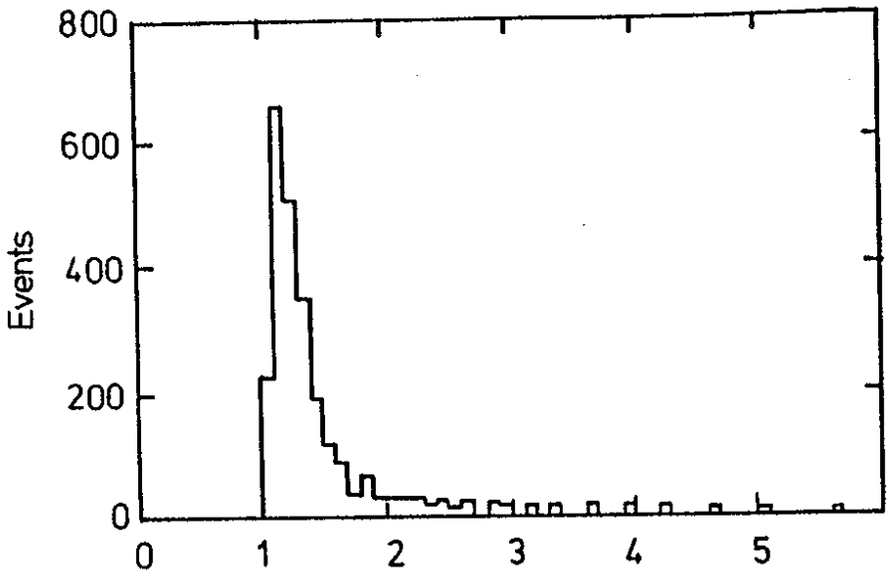

(a) Acceptance Weight

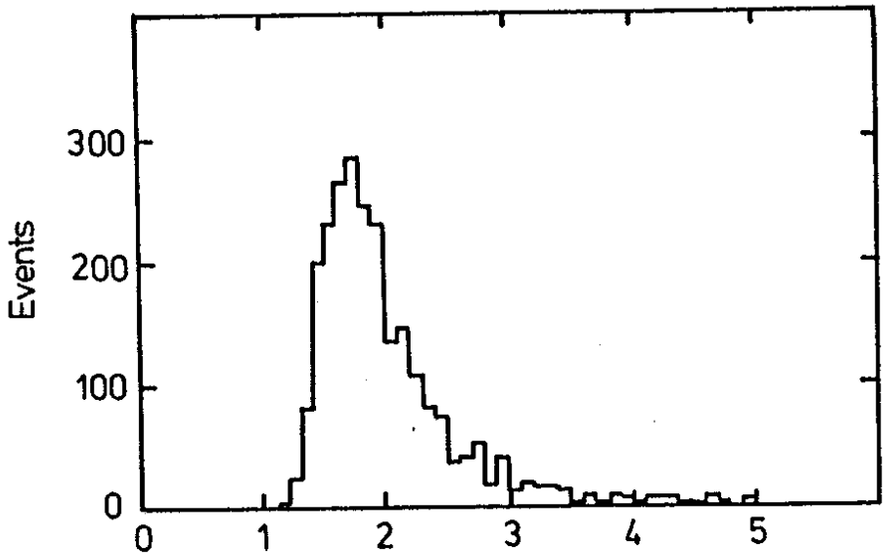

(b) Reconstruction Weight

Fig. 4

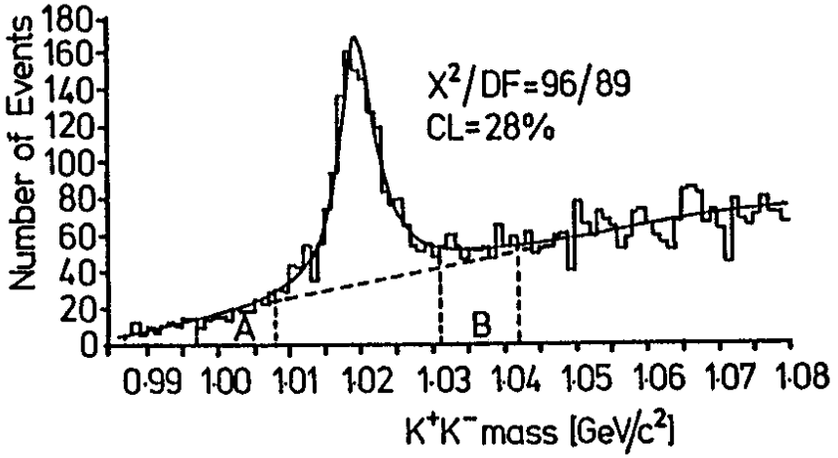

Fig. 5

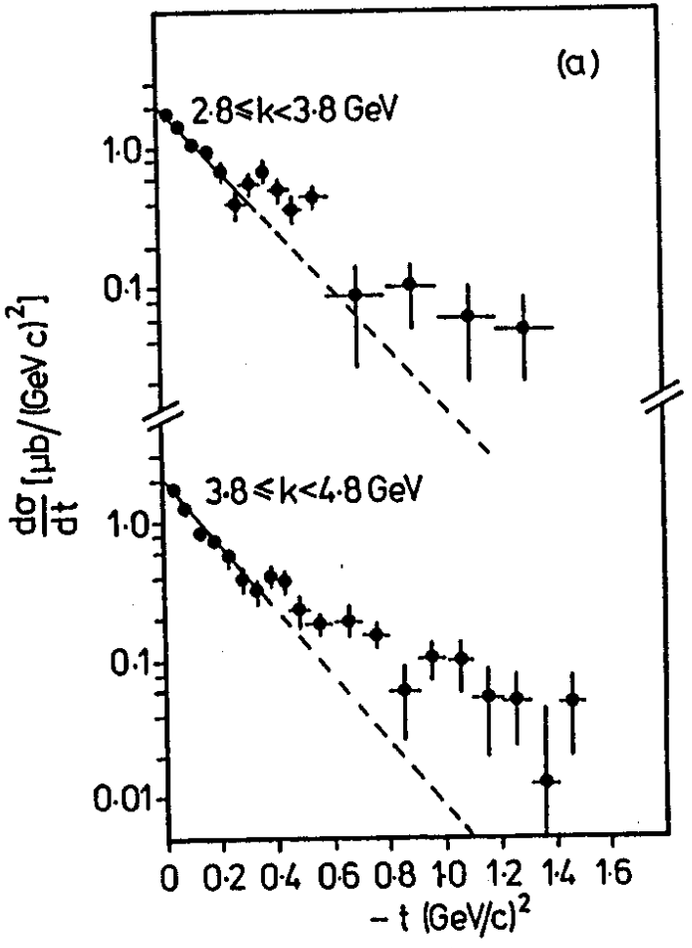
(a)
2·8≤k<3·8 GeV
3·8≤k<4·8 GeV
1·0
0·1
0·01
dσ/dt [μb/(GeV c)²]
0 0·2 0·4 0·6 0·8 1·0 1·2 1·4 1·6
– t (GeV/c)²

Fig.6a

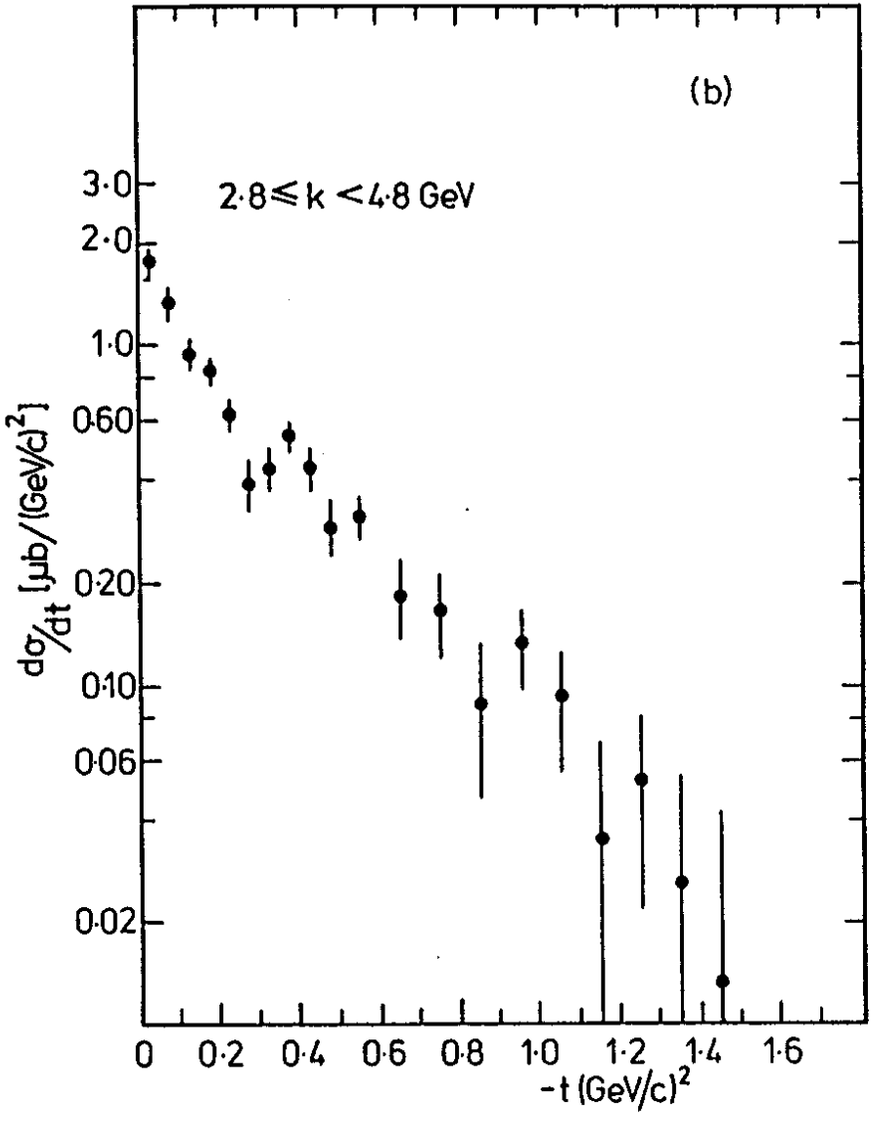
(b)
2·8≤k<4·8 GeV
3·0
2·0
1·0
0·60
0·20
0·10
0·06
0·02
dσ/dt [μb/(GeV/c)²]
0 0·2 0·4 0·6 0·8 1·0 1·2 1·4 1·6
-t (GeV/c)²

Fig. 6b

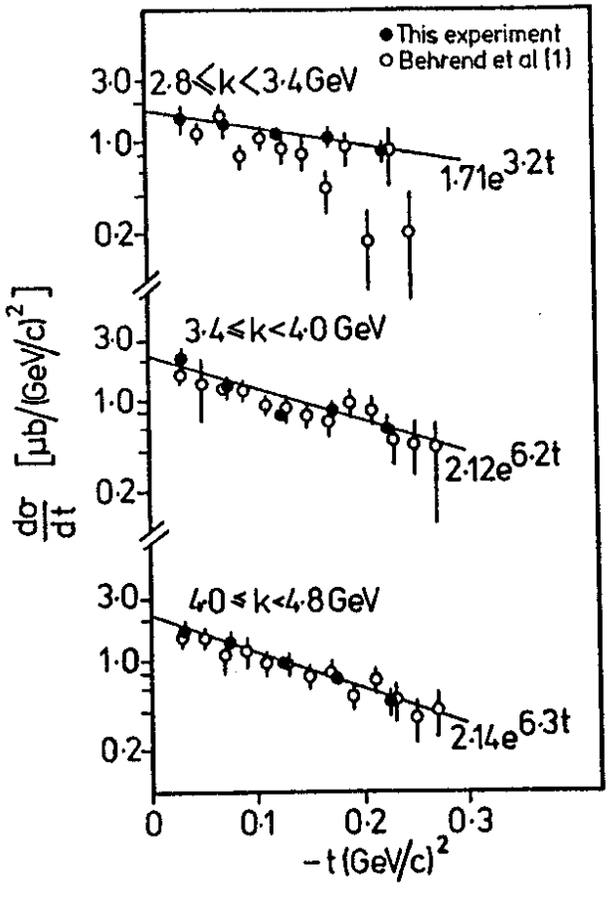
● This experiment
○ Behrend et al [1]
2·8⩽k<3·4 GeV
1·71e^3·2t
3·4⩽k<4·0 GeV
2·12e^6·2t
4·0⩽k<4·8 GeV
2·14e^6·3t
dσ/dt [μb/(GeV/c)²]
−t (GeV/c)²

Fig. 7

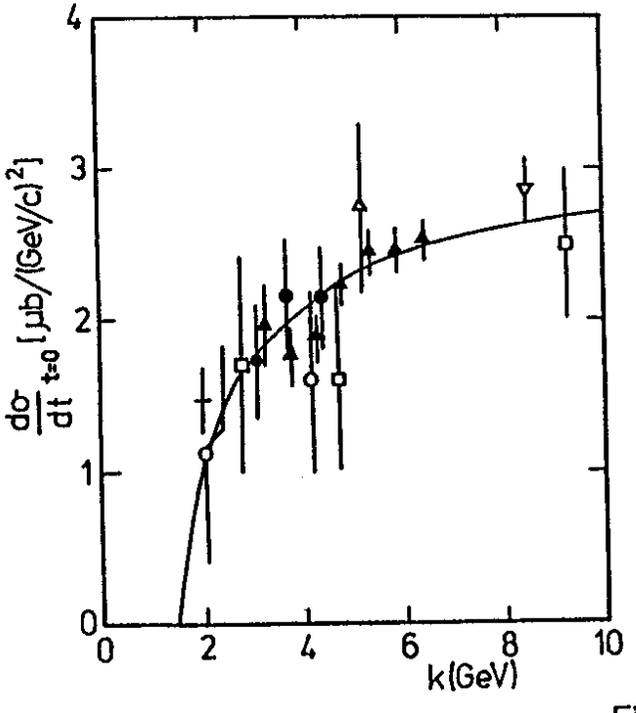
dσ/dt t=0 [μb/(GeV/c)²]
k(GeV)

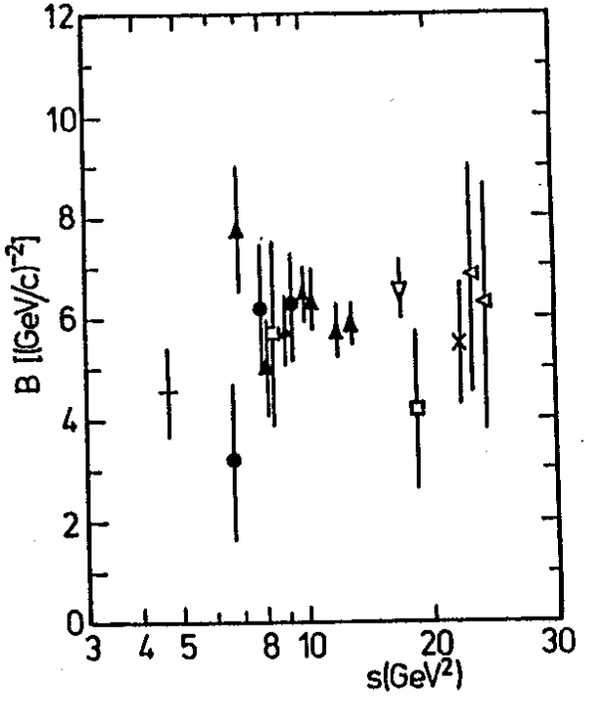
B [(GeV/c)⁻²]
s(GeV²)

Fig. 8

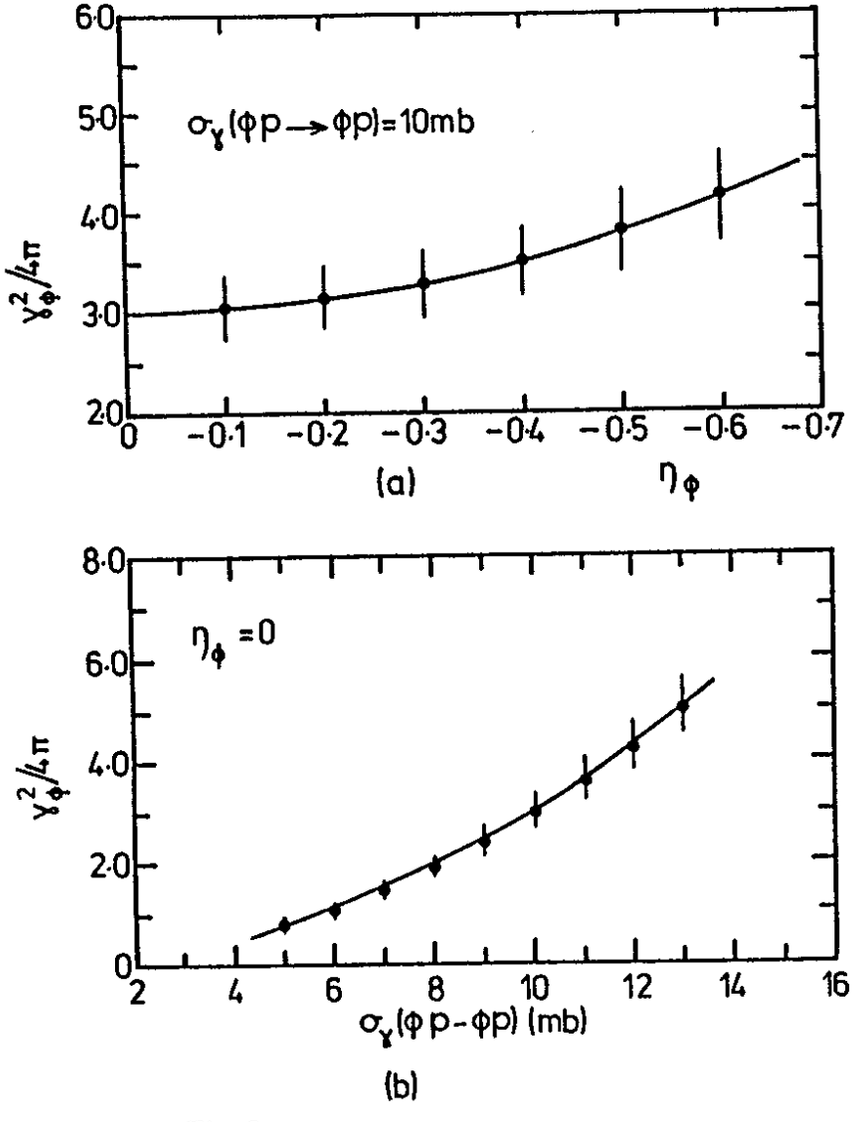
$\sigma_\gamma(\phi p \to \phi p) = 10mb$
$\gamma_\phi^2/4\pi$
η_ϕ
(a)
$\eta_\phi = 0$
$\sigma_\gamma(\phi p - \phi p)$ (mb)
(b)

Fig. 9

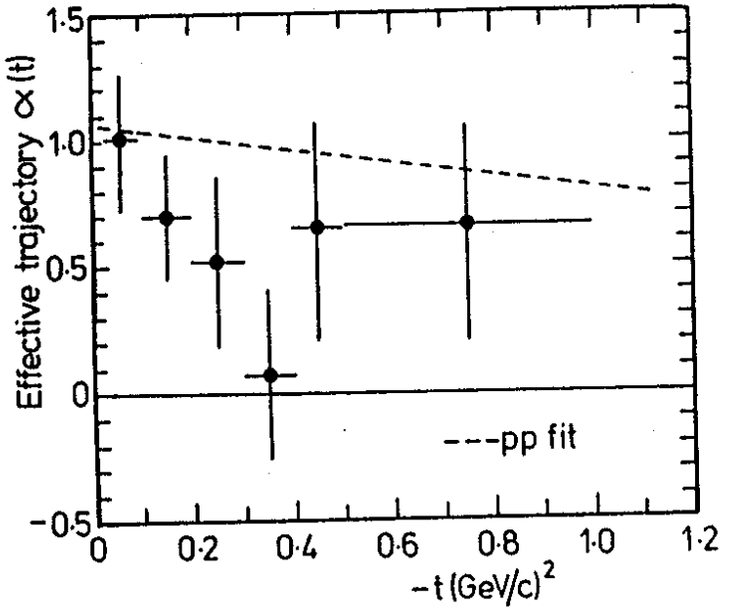
Effective trajectory $\alpha(t)$
---pp fit
$-t$ (GeV/c)^2

Fig. 10

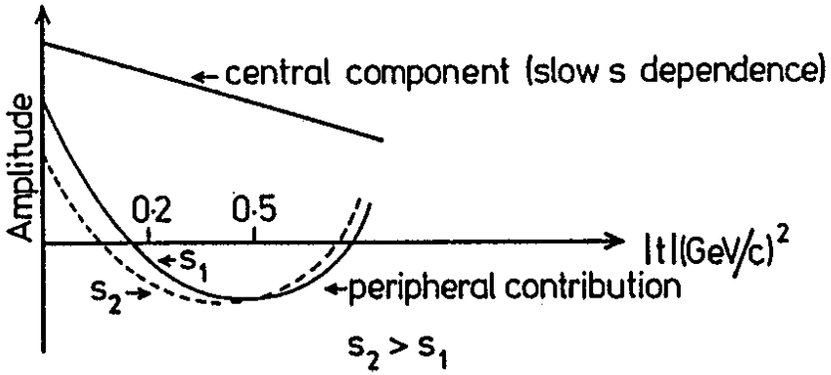
central component (slow s dependence)
Amplitude
0·2
0·5
|t|(GeV/c)²
s₁
s₂
peripheral contribution
s₂ > s₁

Fig. 11

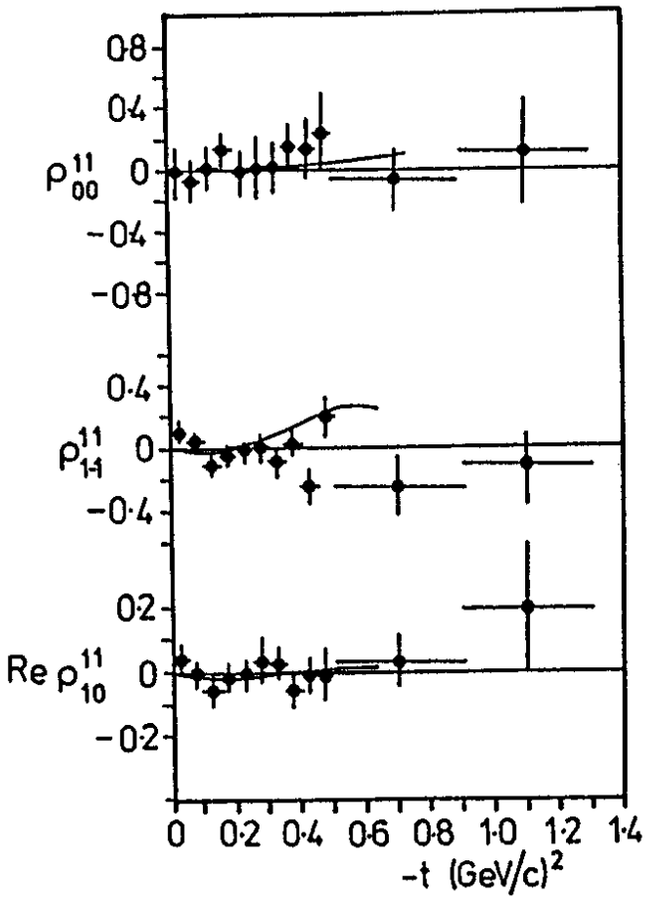
0·8
0·4
ρ¹¹₀₀ 0
-0·4
-0·8
0·4
ρ¹¹₁₋₁ 0
-0·4
0·2
Re ρ¹¹₁₀ 0
-0·2
0 0·2 0·4 0·6 0·8 1·0 1·2 1·4
-t (GeV/c)²

Fig. 12

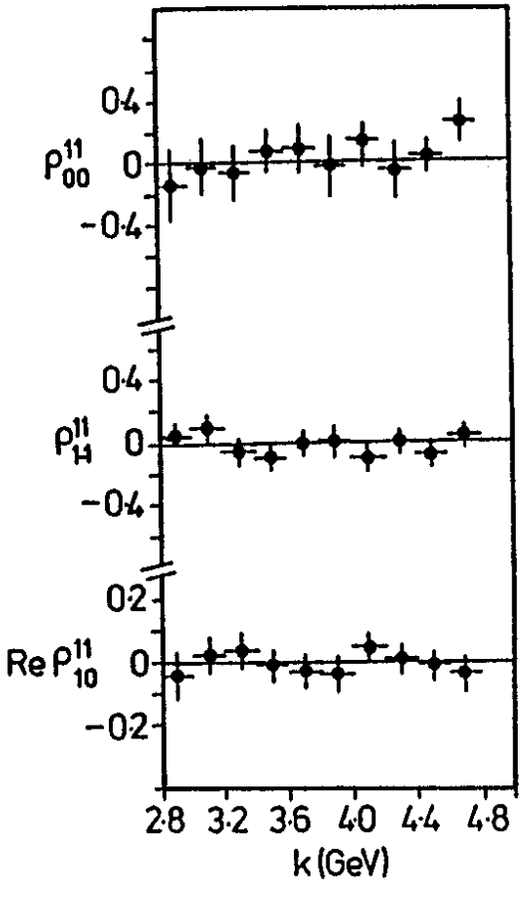
0·4
ρ_{00}^{11} 0
−0·4
0·4
ρ_{1-1}^{11} 0
−0·4
0·2
Re ρ_{10}^{11} 0
−0·2
2·8 3·2 3·6 4·0 4·4 4·8
k (GeV)

Fig. 13

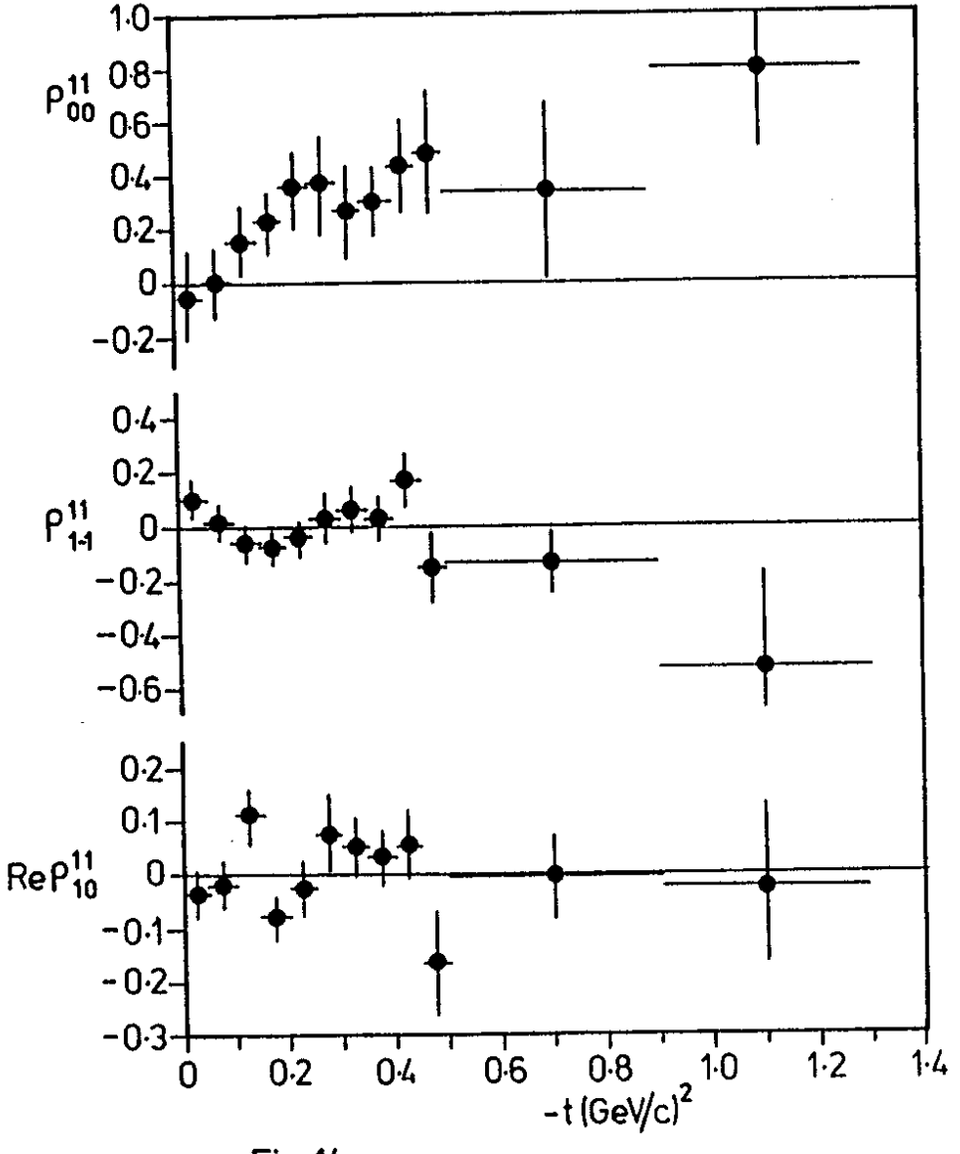
1·0
ρ_{00}^{11} 0·8
0·6
0·4
0·2
0
−0·2
0·4
0·2
ρ_{1-1}^{11} 0
−0·2
−0·4
−0·6
0·2
0·1
Re ρ_{10}^{11} 0
−0·1
−0·2
−0·3
0 0·2 0·4 0·6 0·8 1·0 1·2 1·4
−t (GeV/c)^2

Fig. 14

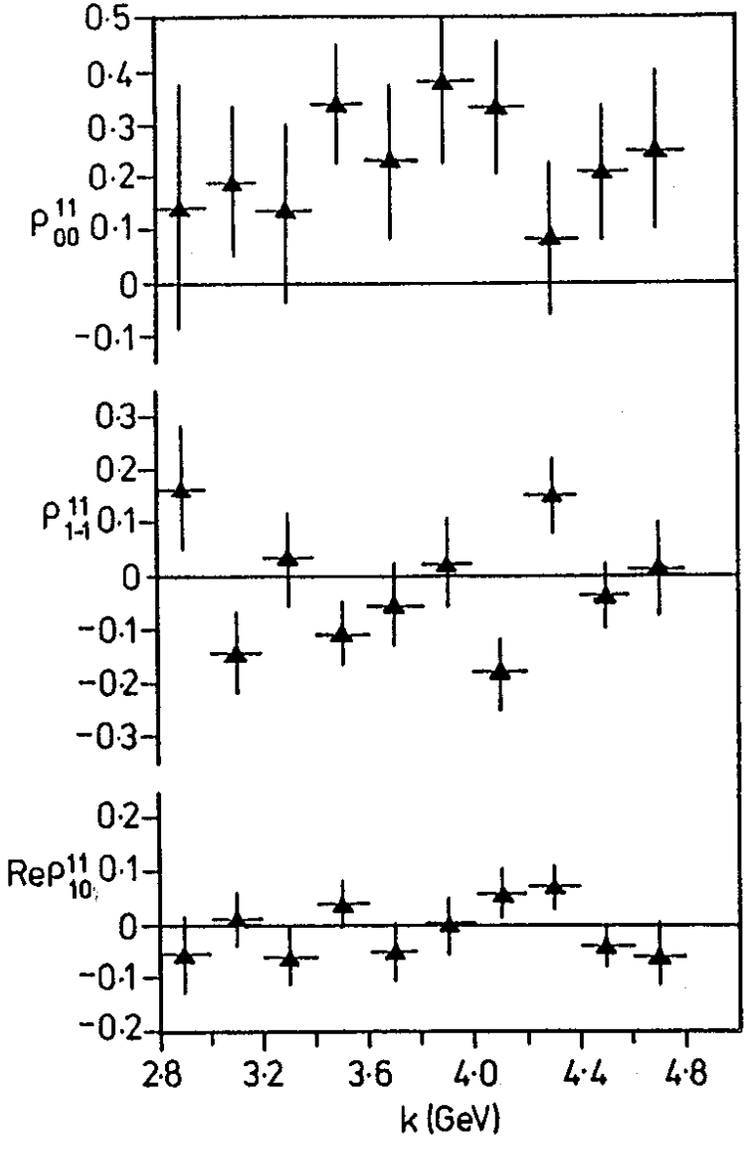

Fig. 15

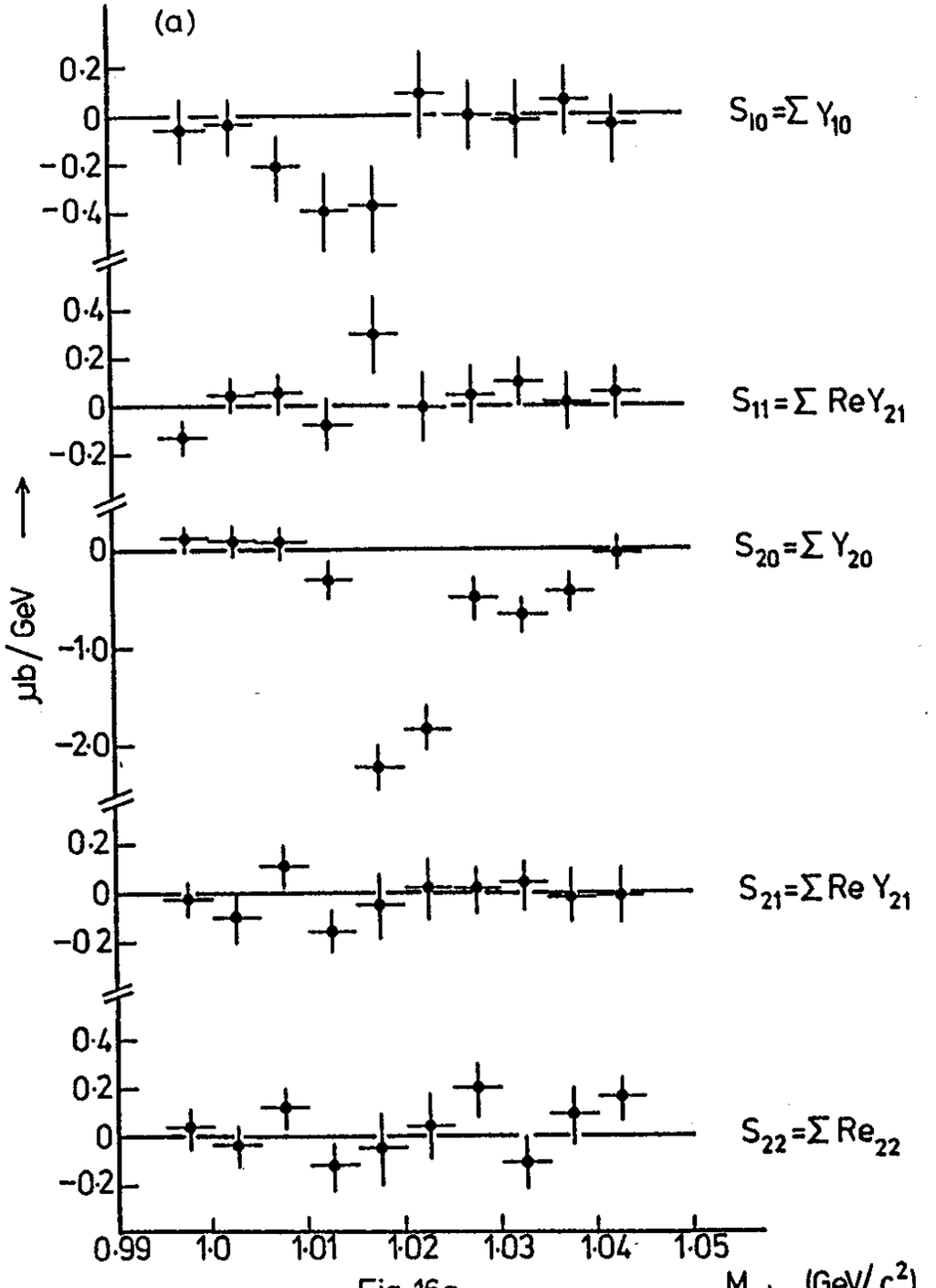

Fig. 16a

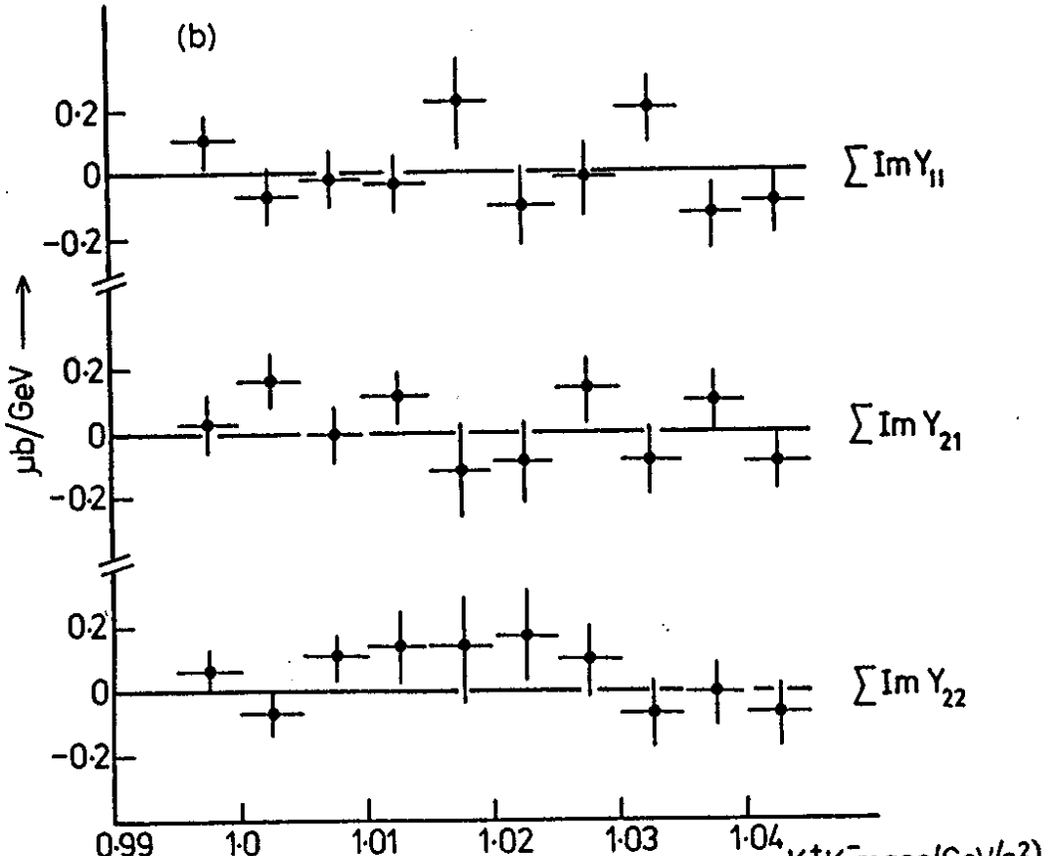

Fig. 16b

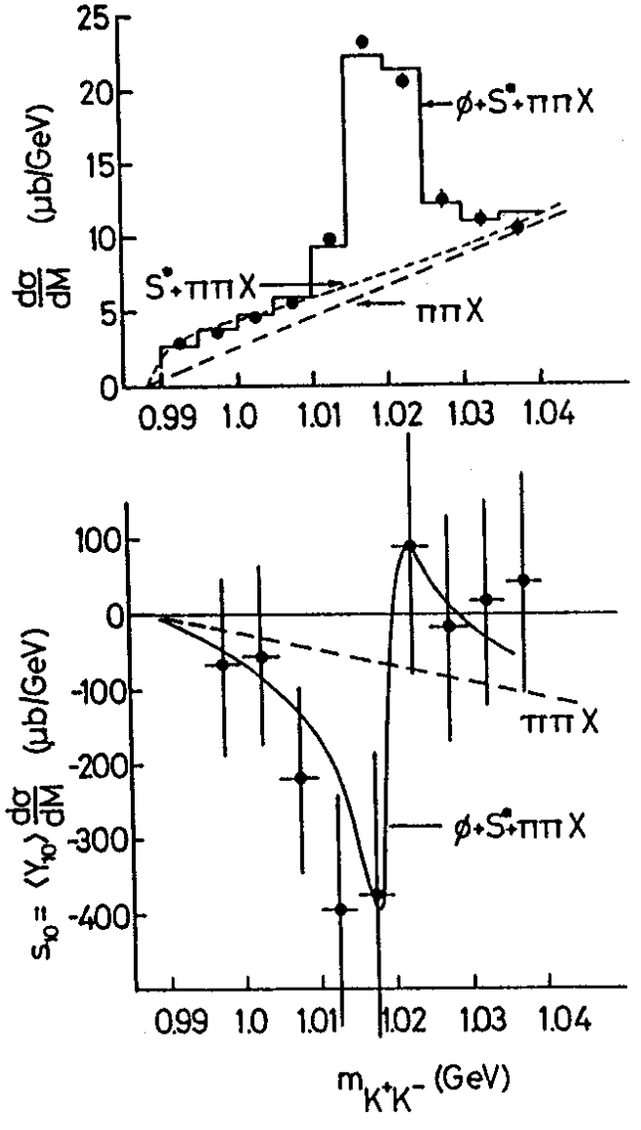

Fig. 17a

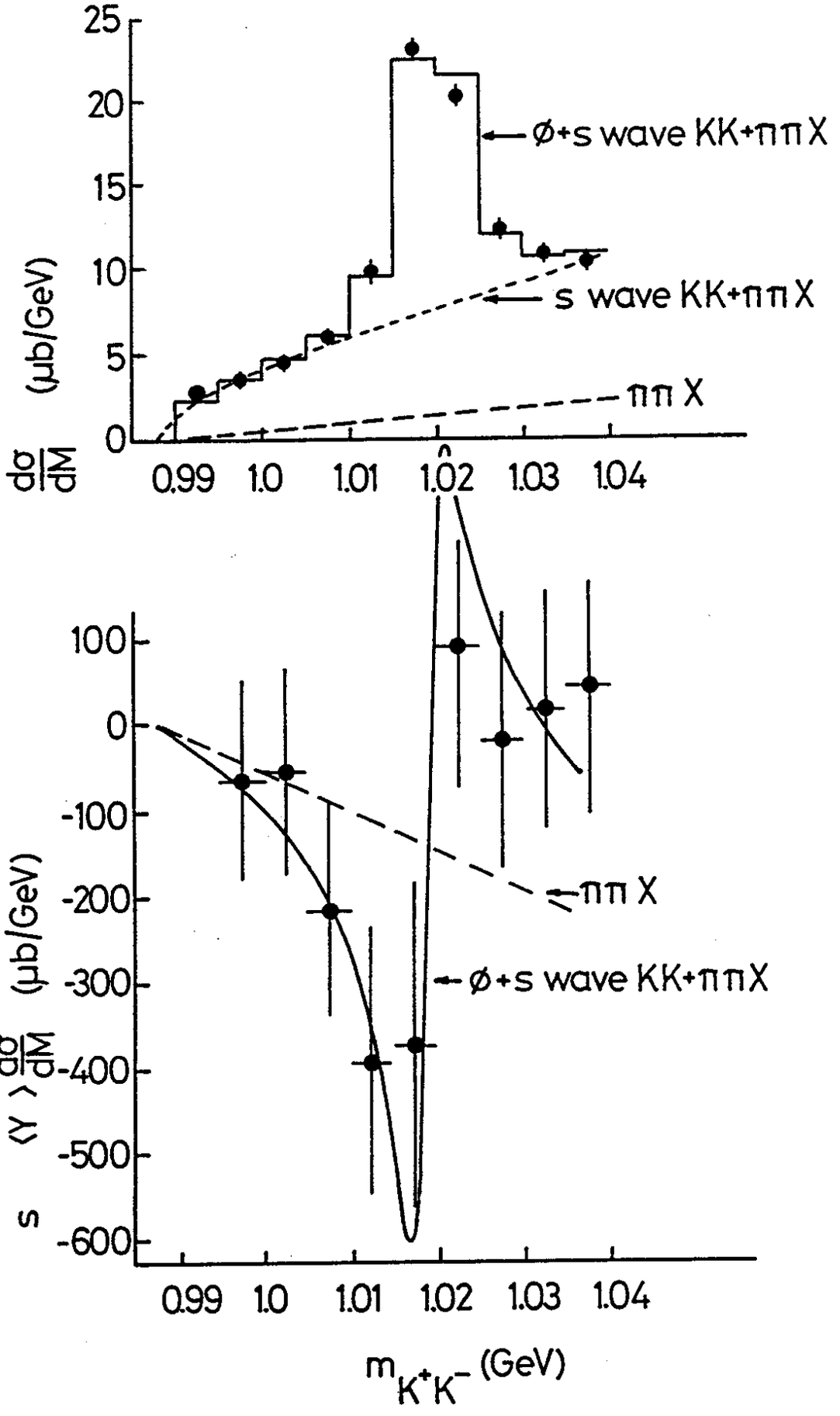
25
20
15
10
5
0
dσ/dM (μb/GeV)
Ø+s wave KK+ππX
s wave KK+ππX
ππX
0.99
1.0
1.01
1.02
1.03
1.04
100
0
-100
-200
-300
-400
-500
-600
s ⟨Y⟩ dσ/dM (μb/GeV)
ππX
Ø+s wave KK+ππX
m K+K− (GeV)

Fig. 17b